

Revealing Surface Changes in a Transparent Gallium Air Battery



A Major Qualifying Project Report

Submitted to the Faculty of the

Worcester Polytechnic Institute

in partial fulfillment of the requirements for the

Degree of Bachelor of Science

In

Chemical and Mechanical Engineering

Submitted by:

Donald Coley

Shayne Barton

Nicole Bodinizzo

Date: May 6, 2021

Advisors: Andrew Teixeira

Pratap Rao

This report represents the work of WPI undergraduate students submitted to the faculty as evidence of completion of a degree requirement. WPI routinely publishes these reports on its website without editorial or peer review. For more information about the project program at WPI, please see <http://www.wpi.edu/academics/ugradstudies/project-learning.html>

Acknowledgments:

If not for the undeniable help and support from others, this project would not be achievable. A special thanks goes out to the following people for their contributions to our project:

- **Professor Andrew Teixeira**, for offering his lab space and equipment for us to use and for answering all our questions and providing helpful information during our discussions.
- **Professor Pratap Rao**, for providing our team with essential materials for our research and for offering helpful feedback during our discussions.
- The graduate student(s): Cameron Armstrong, Ari Athair, and Jacob Crislip for supporting our team throughout the year and providing help with lab equipment.
- **Worcester Polytechnic Institute**, for supporting our team's research into transparent air-metal batteries as well as keeping our campus safe and clean during the global pandemic.

Abstract

To account for the increasing demand for energy, we need to discover the next advancement in clean energy. When compared to its commercially available counterpart Zinc, Gallium boasts 150% the theoretical energy density Zinc has and can introduce liquid kinetics at reasonable temperature ranges. Previous MQPs have tried using a liquid gallium anode battery configuration with promising results in a Swagelok configuration. This project looked to identify the mechanisms for failure within the liquid metal-air battery configuration in a transparent and semi-flexible configuration. The goal was to design and construct a lab test cell battery to visualize the electrochemical reaction during charge and discharge. The resulting studies highlight the self-actuating movement during charge and discharge due to the gallium oxide-gallium surface tension interface. The major findings of this study were: 1) the effects of gallium oxide formation in thin interfaces, 2) electrolysis can hinder the rechargeability of the cell with a liquid electrolyte, 3) rechargeability of the cell is dependent on the maintenance of KOH electrolyte in the configuration.

Authorship Page

Section Primary	Author
Abstract	All
1.0 Introduction	All
1.1 The Modern Battery	Nicole
1.2 Metal-Air Batteries	Nicole, Donald
1.2.1 Liquid metal's characteristics and its application in batteries	Shayne, Donald
1.2.2 The case for gallium	Shayne, Donald
1.2.3 Liquid batteries faster kinetics	Nicole, Donald
1.3 The case for Flexible batteries	Shayne, Donald
1.4 What we can learn from Micro Batteries	Nicole, Donald
1.5 The properties of Microfluidic Batteries and their potential applications	Nicole
1.6 Motivations for this project	Shayne, Donald
2.0 Literature Review	All
2.1 Lithium-Ion Batteries	Donald
2.2 Zinc-Air Batteries	Donald
2.3 Separator Issues	Donald
2.4 Liquid batteries	Donald
2.4.1 LMBs as Aluminum Refinement Cells in the 1900s	Donald
2.4.2 LMBs with both metal cathode and anode	Donald
2.5 Gallium Anode	Donald
2.5.1 Phase Diagram of Gallium	Nicole
2.5.2 Materials that Will not Alloy with Gallium	Nicole
2.6 Previous Relevant Work	Nicole

2.6.1 Work Achieved by 2015 MQP	Nicole
2.6.2 Work Achieved by 2016 MQP	Nicole
2.6.3 Work Achieved by 2017 MQP	Nicole
2.6.4 Work Achieved by 2020 MQP (Latest)	Nicole
2.6.5 Gough Paper	Shayne
2.6.6 “Soft, Highly Elastic...Metal-Air Battery”	Donald
3.0 Methodology	Nicole, Donald
3.1 Recreating Gough Configuration	Nicole, Donald
3.2 Materials	Nicole, Donald
3.2.1 Material Differences	Donald
3.2.2 Aluminum Inclusion	Donald
3.3 Battery Analyzer	Nicole, Donald
3.3.1 Tests on Gough Configuration	Nicole, Donald
3.3.2 The GaNTS cell, its differences to 2020 MQP and proposed tests	Donald
3.4 Image and Video and image processing Software	Donald
3.4.1 ImageJ	Donald
3.4.2 USB Celestron Microscope	Donald
4.0 Results	All
4.1 Our Gough Configuration results without aluminum	Donald
4.2 Anodic Reactions in both Reservoirs A and B	Donald
4.3 Cathodic Reactions in both Reservoir A and B	Donald
4.4 Making the GaNTS Cell	Donald
4.4.1 Determining the GDL	Donald
4.4.2 Gel Electrolyte	Donald
4.4.3 Module Resistance	Donald
4.4.4 Building Our Final GaNTS cell	Donald
4.4.5 Comparing Polarizations over a longer range of Current	Donald
4.5 Discharge Cycle	Nicole
4.5.1 Our Best Discharge Results	Nicole
4.5.2 Reproducibility of Our Discharge Curve	Nicole
4.5.3 Discharge curve of GaNTS cell using NaOH Electrolyte	Nicole

4.5.4 Orphaning withing the GaNTS Configuration	Nicole
4.6 Discharge-Charge Cycles	Nicole
4.6.1 Testing for Rechargeability and Stability	Nicole
4.6.2 Testing with a Stainless-Steel Electrode	Nicole
4.7 Charge Cycle and Gallium Production	Shayne
4.7.1 Control Test (Water Only)	Shayne
4.7.2 Control Test (KOH Only)	Shayne
4.7.3 Gallium Oxide dissolved into KOH Electrolyte (1 mA)	Shayne
4.7.4 Gallium Oxide dissolved into KOH Electrolyte (5 mA)	Shayne
5.0 Conclusions and Future Work	All
5.1 Complications with Materials: Feasibility of the Configuration	Donald
5.1.1 Leakage liquid electrolyte + polyimide	Nicole
5.1.2 Electrode slipping/deformation polyimide tape	Nicole
5.2 Complications during Reproducibility	Nicole
5.2.1 Required New Parts Each Test (or reusing)	Shayne
5.2.2 Use of Gallium Required an Incubator	Shayne
5.3 Working during COVID-19	Nicole
6.0 Future Work	Nicole

Table of Contents

Revealing Surface Changes in Transparent Gallium Air Battery	1
Acknowledgments:.....	2
Abstract	3
Authorship Page.....	4
List of Figures	10
List of Tables	13
1. Introduction.....	14
1.1 The Modern Battery	14
1.2 Metal-Air Batteries	14
1.2.1 Liquid metal's characteristics and its application in batteries	16
1.2.2 The case for gallium	16
1.2.3 Liquid batteries faster kinetics.....	17
1.3 The case for Flexible batteries.....	18
1.4 What we can learn from Micro Batteries.....	18
1.5 The properties of Microfluidic Batteries and their potential applications	19
1.6 Motivations for this project.....	20
2. Literature review	22
2.1 Lithium-Ion Batteries.....	23
2.2 Zinc-Air Batteries	24
2.3 Limitations in separator technology.....	25
2.4 Liquid metal batteries.....	26
2.4.1 Aluminum Refinement Cells in the 1900s.....	27
2.4.2 LMBs with both metal cathode and anode.....	28
2.5 Gallium's reversible oxide formation	31
2.5.1 Phase Diagram of Gallium	32
2.5.2 Materials that Will not Alloy with Gallium.	34
2.6 Previous Relevant Work.....	35
2.6.1 Work Achieved by 2015 MQP	36
2.6.2 Work Achieved by 2016 MQP	37
2.6.3 Work Achieved by 2017 MQP	39
2.6.4 Work Achieved by 2020 MQP (Latest)	41

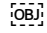
2.6.5 Gallium and its redox reaction powered self-actuation	43
2.6.6 “Soft, Highly Elastic, and Discharge-Current-Controllable Eutectic Gallium Indium Liquid Metal-Air Battery”	46
3. Methodology	51
3.1 Baseline performance with the Gough Configuration	51
3.2 Materials	52
3.2.1 Material Differences	53
3.2.2 Aluminum Inclusion	55
3.3 Battery Analyzer	56
3.3.1 Tests on Gough Configuration	56
3.3.2 The GaNTS cell, its differences to 2020 MQP, and the proposed tests	57
3.4 Video and Image Processing	58
3.4.1 ImageJ	58
3.4.2 USB Celestron Microscope	59
4. Results	60
4.1 Our Gough Configuration results without aluminum	60
4.2 Anodic Reactions in both Reservoirs A and B	61
4.3 Cathodic Reactions in both Reservoir A and B	62
4.4 Making the GaNTS Cell	64
4.4.1 Determining the GDL	64
4.4.2 Gel Electrolyte	65
4.4.3 Module Resistance	66
4.4.4 Building Our Final GaNTS cell	67
4.4.5 Comparing Polarizations over a longer range of Current	68
4.5 Discharge Cycle	69
4.5.1 Our Best Discharge Results	69
4.5.2 Reproducibility of Our Discharge Curve	71
4.5.3 Discharge curve of GaNTS cell using NaOH Electrolyte	72
4.5.4 Orphaning withing the GaNTS Configuration	73
4.6 Discharge-Charge Cycles	74
4.6.1 Testing for Rechargeability and Stability	74
4.6.2 Testing with a Stainless-Steel Electrode	78
4.7.1 Control Test (Water Only)	79
4.7.2 Control Test (KOH Only)	81

4.7.3 Gallium Oxide dissolved into KOH Electrolyte (1 mA).....	83
4.7.4 Gallium Oxide dissolved into KOH Electrolyte (5 mA).....	84
5.0 Conclusions & Recommendations.....	86
5.1 Complications with Materials: Feasibility of the configuration	86
5.1.1 Leakage liquid electrolyte + polyimide	86
5.1.2 Electrode slipping/deformation polyimide tape	87
5.2 Complications during Reproducibility.....	88
5.2.1 Required New Parts Each Test (or reusing).....	88
5.2.2 Use of Gallium Required an Incubator.....	89
5.3 Working During Covid.....	90
6.0 Future Work.....	91
References.....	92
Appendix A: Noteworthy Videos.....	95
Appendix B: Incubator Setup	97
Appendix C: Assembling Gough Module	99
Appendix D: Miscellaneous Calculations	101
Appendix E: Materials Purchased	103

List of Figures

Figure 1. Metal-Air Battery Configuration showing how Oxygen from the outside powers the chemical reactions on the metal and air electrodes.[6]	15
Figure 2. Properties of Gallium based liquid metals. [8]	17
Figure 3. Microfluidic Battery Configuration highlighting the dual-pass flow [5]	20
Figure 4. Stanley Whittingham's battery configuration [27]	24
Figure 5. Liquid Metal Battery Configuration [15]	26
Figure 6. Hoopes and Betts Liquid Metal Battery Configurations [16].....	28
Figure 7. Liquid Metal battery configuration with molten salt electrolyte [14]	29
Figure 8. Deposition potentials of candidate metals [14]	30
Figure 9. Phase Diagram of Gallium with respect to Temperature and Pressure [21]	32
Figure 10. Phase Diagram of Gallium and Copper [22]	33
Figure 11. Phase diagram of Gallium and Tungsten showing a much more favorable electrode than copper shown in Figure 10 [23]	34
Figure 12. Potential Gallium-air battery flow configuration [20].....	38
Figure 13. “Duck” shape voltammogram curve which indicated reversibility [35]	42
Figure 14. The process of Galvanic actuation between the two reservoirs [19]	45
Figure 15. Cable-shaped eutectic gallium-indium liquid metal-air battery. A) highlights the methodology for creating the battery and b) shows the components and characteristics of elasticity and flexibility [29]	47
Figure 16. Oxygen reduction rate improvement from Pt catalyst coating [29]	48
Figure 17. Open-ended battery configuration of the EGILM and carbon fiber yarn cell [29]	48
Figure 18. Effects on the discharge current of the cable-cell a) highlights the effect of injection % b) highlights the effect of truncation c) highlights the effects of twisting and d) highlights the effects of stretching [29]	50
Figure 19. Gough Configuration Design made in Solidworks.....	52
Figure 20. Galinstan droplet preparation inside of a Self-Actuation test module.....	54
Figure 21. Left Current and Speed Results from Gough Experiments. Right Circuit diagram showing flow of current in relation to the image of the system in the graph to the left.[19]	56
Figure 22. Comparing our final GaNTS Design to 2020 MQP Swagelok Cell	58

Figure 23. Reservoirs A and B in the Gough configuration for visualizing self-actuation	60
Figure 24. Our results when reproducing the Gough paper self-actuation test. The results are comparable to the published results found in Figure 21	61
Figure 25. Air formation in Reservoir B	63
Figure 26. The photos above show the copper oxide formation in the electrode helping to deduce the flow of electrons.....	63
Figure 27. Expanded Module with Tungsten Electrode connection to Cathode	64
Figure 28. Comparing GDL polarization performance.....	65
Figure 29. Gel Electrolyte preparation.....	66
Figure 30. Comparing the Effects with and without the Gel Electrolyte to Commercial-Grade Zinc-Air Battery	66
Figure 31. Voltage and Resistance check with new Configuration.	67
Figure 32. Comparing polarization to Swagelok configuration.....	68
Figure 33. <i>Comparing Polarizations for reproducibility. Left shows the current density if the surface area is considered the total surface area of the gallium droplet due to the no slip boundary clause Right shows the current density calculation if we consider that ion transfer of gallium happens only along the boundary of gallium and the separators.</i>	69
Figure 34. GaNTS cell discharge curve at 50 °C and 2.45 mA/cm ²	70
Figure 35. Showing Reproducibility of the Results of our best discharge curves both run at 0.5 mA.....	71
Figure 36. Left. Before and Right. After 4.5-hour discharge from 3/15/21	71
Figure 37. Discharge curve using NaOH electrolyte. NaOH electrolyte was able to run slightly longer before failing but displayed instability throughout the test run.	72
Figure 38. Discharge curve for 4/1/21 run. The circled area above indicates where we believed chemical orphaning was taking place. See Appendix A Video 3 to view this test run.	73
Figure 39. Failed Discharge/Charge Test on Second Discharge cycle. Pictures A. , B. , and C. : Change in contact area between Gallium and separators (anode and cathode) shows failure method. Liquid KOH Electrolyte evaporation shown by receding liquid front on the Tungsten Electrode and in layers of polyimide between images B. and C.	75
Figure 40. Discharge/Charge cycle at 5 mA current with 30-minute intervals. Each picture represents the start of a cycle and shows the differences overtime.	76

Figure 41. Potential vs. time graph for discharge/charge. Left. 2020 cell Right. GaNTS cell ...	77
Figure 42. Comparing the Charge Cycles from the 03/17/2021 Discharge-Charge Test	78
Figure 43. Program report of discharge/charge test for cell with SSE	79
Figure 44. Example of petri dish configuration	80
Figure 45. Shows the voltage and current vs time for the water only test.	81
Figure 46. Left. shows the tungsten electrode from water only test just after program began.	
Right shows the tungsten electrode from water only test as program is about to end	81
Figure 47. Shows the voltage and current vs. time of the KOH only charge test	82
Figure 48. Left. tungsten electrode from KOH only test after program began. Right. tungsten electrode from water only test as program is about to end	82
Figure 49. Voltage and Current Vs. Time Graph of 1 mA Ga ₂ O ₃ in KOH Charge Test.....	83
Figure 50. Shows the voltage vs. time for the water only, KOH only, and 0.001 mol Ga ₂ O ₃ in KOH charge tests	83
Figure 51. Left. Shows tungsten electrode at beginning of charge cycle. Right. Shows tungsten electrode at the end of the charge cycle	84
	
Figure 53. Shows the gallium recovered from 5 mA gallium oxide dissolved in KOH electrolyte charge test	85
Figure 54. Leakage after running a few cycles	86
Figure 55. Evidence of KOH leakage through the polyimide layers	88
Figure 56. Shows the disintegrated separators due to long-term KOH exposure	89

List of Tables

Table 1. Open Circuit Voltage for Gallium Hydroxide Product [34]	39
Table 2. Open Circuit for Gallium Oxide Product [34]	40
Table 3. Reactions of the EGILM-air battery [29]	49
Table 4. Table of Resistances inside Module	66

1. Introduction

1.1 The Modern Battery

Lithium-ion batteries have revolutionized the battery industry and have been the cause of many advancements in technology. The revolution of lithium-ion batteries began in the early 1990s when Sony and several other companies released the first commercialized version of this new battery technology [1]. Since then, there have been extensive improvements and countless research to enhance the performance of LIBs. Nowadays, LIBs are the default choice for most personal electronics, including smartphones, laptops, tablets, and electric vehicles. Utilizing lithium-based batteries brings many advantages that have the power to change the world. High energy density, limited maintenance level, long cycling performance, and the ability to self-discharge are the significant benefits of this technology [2]. However, there are some shortcomings of LIBs that need to be improved. First, the lithium metal electrode can develop dendrites that lead to the short-circuiting of the battery. Additionally, LIBs have the potential to catch fire or explode if damaged [2]. Although the advantages of lithium-ion based batteries outweigh the issues, innovations in the battery industry may be able to exceed LIB performance.

1.2 Metal-Air Batteries

According to recent research, an increase of 30% at most in energy density can be made for lithium-ion batteries technology. This indicates that conventional lithium-ion technology is approaching its upper limit for performance [6]. Therefore, the need for new battery configurations is essential for the continuous advancements in both the battery and technology industries. A promising configuration which has gained much research interest as an energy storage technology in consumer electronic products is a metal-air battery. Metal-air batteries are recognized as hybrid

of batteries and fuel cells due to its ability to utilize oxygen from the atmosphere at the cathode as seen in figure 1[6]. These batteries have high theoretical energy densities in the range of 1353-11429 Wh kg⁻¹, which is 3-30 times higher than that of a lithium-ion battery [6]. In a conventional metal-air battery there consists of a metal anode saturated with an electrolyte, a porous air cathode which absorbs the surrounding air, and a separator which mechanically disconnects the cathode from the anode. Zn-, Al-, Mg-, and Li-air are all common types of metal-air batteries that show promising electrochemical performances and long-term stability. Metal-air batteries have many intrinsic advantages over a conventional LIB, including the usage of abundant raw materials, low cost, high safety, and environmental friendliness [6]. However, one major limitation of these batteries which needs additional improvements is their tendency to oxidize which burns out the electrolyte.

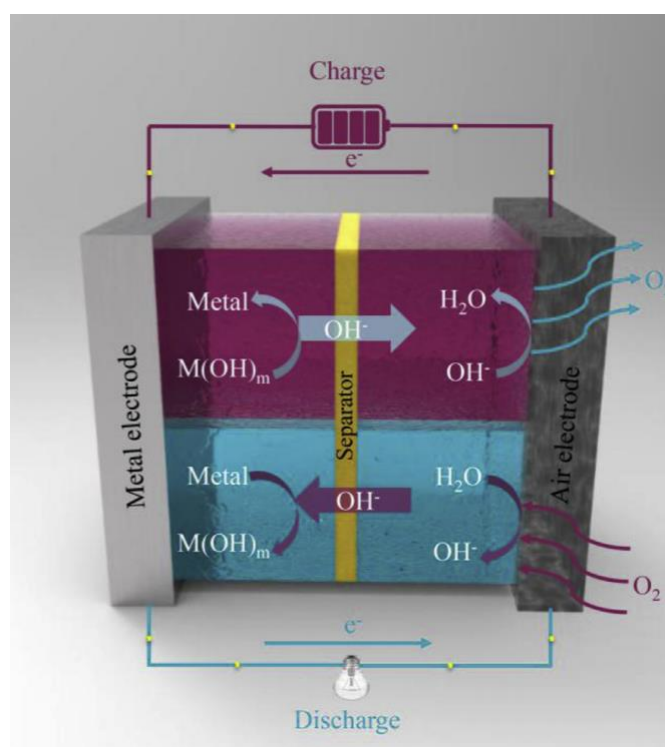


Figure 1. Metal-Air Battery Configuration showing how Oxygen from the outside powers the chemical reactions on the metal and air electrodes.[6]

1.2.1 Liquid metal's characteristics and its application in batteries

Metals in their liquid state enjoy numerous unique qualities and characteristics that their solid counterparts do not have. Besides being a liquid at or near room temperature, liquid metals are highly conductive both thermally and electrically. Due to their liquid nature, liquid metals experience high viscosity and surface tension. Gallium-based liquid metals such as the eutectic GaIn (75% gallium and 25% indium) and Galinstan (68.5% gallium, 21.5% indium, and 10% tin) have emerged in recent years as a non-toxic alternative to mercury [17]. Because of liquid metal's unique combination of high thermal and electrical conductivity as a metal yet deformable as a liquid, gallium-based liquid metal alloys are being utilized in application areas like soft electronics, sensing, microfluidics, reconfigurable radio frequency (RF) devices, and energy harvesting [17]. Most liquid metals are known to oxidize from oxygen in ambient air, forming an ultrathin oxide layer in a self-limiting reaction [7]. When liquid metal is used in battery configurations, it improves the cell's kinetics as is described in detail later.

1.2.2 The case for gallium

The battery's anode must be a good conductor and remain stable throughout the charging and discharging phases of the reaction. To improve the efficiency of the redox reaction, the cell's anode should be a capable reducing agent [26], meaning it readily will give off electron. Gallium provides these key qualities with plenty more favorable traits for the use of an anode. Gallium has a low melting point at 29.7°C, which is just above room temperature. This liquid metal is not particularly dangerous to humans which makes experimentation with this material favorable. Gallium in its liquid state is a great conductor of electricity [8]. Gallium also exhibits a low viscosity which is incredibly important for its application in the Gough configuration as will be illustrated in much more detail later. All gallium-based liquid metal's character traits that make it our preferred material are highlighted in figure 2.

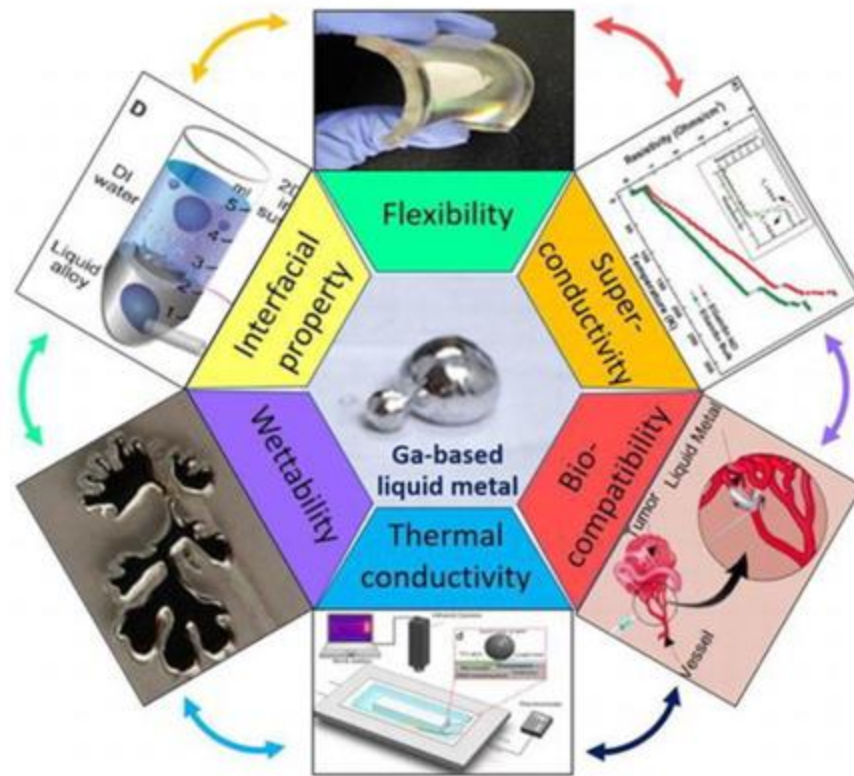


Figure 2. Properties of Gallium based liquid metals. [8]

1.2.3 Liquid batteries faster kinetics

Utilizing a micro battery with liquid kinetics will make for an innovative, innovative battery. Liquid metal batteries have been regarded as a promising energy storage technology typically operated at elevated temperatures to maintain molten-state electrodes and high conductivity of electrolytes. Interestingly, room-temperature liquid metal batteries have made further developments, which show potential as a novel energy system for widespread usage [9]. There are benefits of utilizing liquid metals as electrode materials. First, using liquid metals provides much faster kinetics than typical solid-state electrodes, which satisfy high power demands [9]. By boasting faster kinetics, the reactions that drive the current happen much quicker allowing for a larger power output. Not only that, LMs have a high concentration of electroactive materials, which offers the potential for high capacity and are immune to structural cracks due to its self-

healing capabilities [9]. Additionally, the deformability of room-temperature LMs as an electrode gives the potential to design flexible devices beyond a static system.

1.3 The case for Flexible batteries

In recent years, the research and demand for a battery cell that can perform flexibly have significantly increased. There is currently a 66-billion-dollar sector focusing on the development of flexible, thin, rollable, and foldable [10]. Furthermore, by 2025, 23% of the healthcare market will use flexible batteries [10]. The pairing of a durable high energy density battery with the concept and idea of flexibility has opened a realm of promising applications. One primary application of a non-rigid cell is in wearable technology. Since the battery can withstand external forces such as torsion, tension, and compression while continuing to operate, it would allow it to mount to surfaces expected to move or change. A few noteworthy examples for this battery technology are wearable medical sensors through electric skin patches in hospitals and the health field, flexible energy storage systems, and bendable phone screens such as the Samsung Fold.

1.4 What we can learn from Micro Batteries

Micro-batteries are the advancement of classic lithium batteries and a newer innovation in the battery industry. They offer high voltages, high energy densities, and have a wide working temperature range, making them suitable for a wide range of applications, such as medical equipment and precision instruments. The main difference between a traditional LIB and a micro-battery is that the electrolyte is solid, and thin film vacuum deposition techniques are utilized to achieve thicknesses from 5-20 μm for active layers [3]. These aspects give dramatic advantages, including no risk of leakage or explosion, no self-discharge, high cycling capabilities, retention, high integration capabilities, and the possibility of depositing the battery on various substrates [3]. However, some challenges have prevented the advancement of commercialized micro-batteries,

which will be further discussed in the Literature Review section. One commercially available micro-battery are Zn-air batteries, which are widely used in micro-technologies such as hearing aids. This battery has a layered structure consisting of a zinc anode, an alkaline electrolyte, and an air cathode. Zinc-air batteries not only provide a high energy density, but also produces electrochemical energy by using oxygen, which brings an advantage since oxygen can be directly obtained from the atmosphere [11]. Through various research, this configuration may be used with other metals, such as gallium, to create an advanced innovative battery. Furthermore, the application of a micro battery, more specifically a microfluidic battery, may further innovate the battery industry.

1.5 The properties of Microfluidic Batteries and their potential applications

Microfluidic batteries are the first redox battery to date that does not have a membrane, which capitalizes on dual-pass flow through porous electrodes and operates within a co-laminar flow configuration to generate electrical power [4]. The design is entirely symmetric, which allows for both charging and discharging functions to operate in forward, reverse, and recirculation directions shown in figure 3. Redox flow batteries (RFBs) are an efficient and environmentally safe energy storage system that has gained popularity in the past years. One important quality of these batteries is its ability to separate power generation from energy storage. RFBs demonstrate several advantages over Li-ion batteries, including long-term durability, high round-trip efficiency, and low capital cost [5]. Additionally, microfluidic fuel cell battery configurations have a stacked architecture with multiple functional layers, which this project will apply to utilize liquid kinetics. The use of gallium in a microfluidic configuration may bring benefits to potential applications of these batteries. However, gallium oxide is known to have special microfluidic properties in channels which requires further investigation.

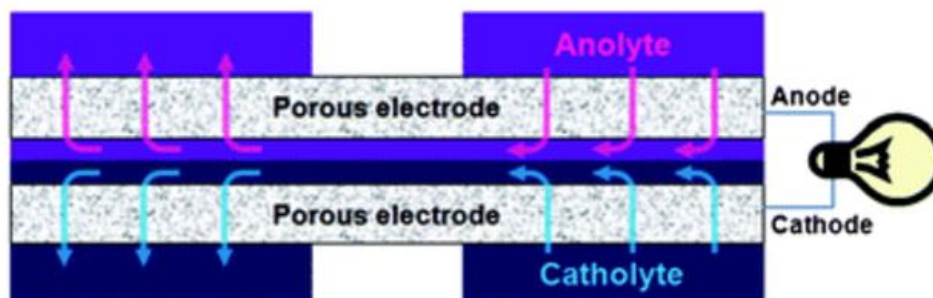


Figure 3. *Microfluidic Battery Configuration highlighting the dual-pass flow [5]*

1.6 Motivations for this project

A realized and functioning flexible micro battery has the potential to change the current market of batteries and their applications. Combining this with how liquid batteries could be structured to support attributes such as flexibility and supporting a small-scale frame, provides a significant connection. Liquid metal-air batteries retain the benefits of a liquid metal battery's faster kinetics and a metal-air battery's higher theoretical energy density yet still supporting the attributes previously named. Because gallium can exist as a liquid metal at just above room temperature, it is a superb conductor and is an excellent choice for the use of an anode.

This project aims to build upon the discoveries from the previous Major Qualifying Projects and apply new techniques and ideas to solve problem areas while hopefully building on the future recommendations they provided. Gallium metal-air batteries have shown great promise in the previous Major Qualifying Projects, and we believed that there was more to be learned from them. We created the battery cell which had the previously unavailable benefit of transparency, explained in more detail in a later section. This allowed us to witness the cell's reactions firsthand and obtain a further understanding of the project's failure points. Our battery cell also had the added benefit of being flexible, opening this new battery technology into previously unobtainable but much wanted areas.

2. Literature review

Most battery cells are made of three main sections, the electrolyte, the anode, and the cathode. For most battery cells, it is the reaction in the anode that drives the battery discharge with valence electrons leaving the metal ions often through a current collector connected to the cathode, while the spent metal ions travel through the electrolyte and any separators present in the cell. Anode is the name for the area where the electrons will transfer from and as such, cathode is where the electrons will go. The choice in electrolyte can be extremely important when looking into optimizing the cell's voltage and rechargeability as it is integral in which anode is chosen. The goal of the electrolyte is to prevent electrode materials from passing if they are neutral but allow them to pass if ionized. While KOH solutions are primarily used as the electrolyte in Zn-air batteries due to excellent ionic conductivity, high oxygen diffusion coefficient, and low viscosity, alkaline electrolytes will cause self-corrosion in Al-air batteries and parasitic hydrogen evolution during battery discharge [6]. The separator is also an area of concern as without the proper separator, the battery can short circuit and experience irreversible damage. In most Swagelok cells for the evaluation of batteries, woven separators dipped in electrolytes are often used in evaluating the electrochemistry of cells. However, non-woven separators have shown improved performance in Ni/Zn systems and hinder dendritic growth of Zn, which is the most common issue facing solid metal batteries [12].

Although some battery cells are cheaper without solid separators, the lack of a solid separator causes the cell to be extremely hard to market for portable applications. Solid separators are known to circumvent the metal dendrite concerns. However, separators are tricky to nail down as these porous separators are required to have a high absorption capacity and appropriate porosity

to sustain electrolytes. Separators trying to use selective transport often result in crossover of soluble metal ions. While some of these parts are omitted from current battery configurations, understanding that each part of the cell is not clear cut but instead needs to be catered to the reaction you want your cell to undergo makes the choosing of proper parts tricky.

For our project we set out to explore the viability of thin film flexible and rechargeable batteries in the hopes of helping to create a new market for batteries as there is already a need for wearable electronics with energy sources which have requirements that can be met by this cell. The sections following will outline the major battery cells seen not only in commercial applications but also in field of research.

2.1 Lithium-Ion Batteries

When one thinks of lithium ions batteries they often think of the batteries in today's smartphones and other portable or other mobile devices. The drive for portable power applications continue to drive research and development of advanced battery systems to new heights and lithium-ion technology has stood at the forefront in commercial application. When compared to other metals, lithium has the lightest weight, highest voltage, and greatest energy density, making it a fantastic option for portable battery applications. Research into the application of lithium in electrochemical applications started in 1958 with a paper by Harris. In his paper, Harris made a note that AlCl_3 and LiAlH_4 when dissolved separately in ether gave a poorly conducting solution, but when mixed, the result is a good conductor which allows for good depositions upon electrolysis [Harris]. The 1970s saw the rise in lithium-ion battery technology with the adoption of this technology first from Stanley Whittingham in the 1970s while working for Exxon. The configuration is shown in figure 4.

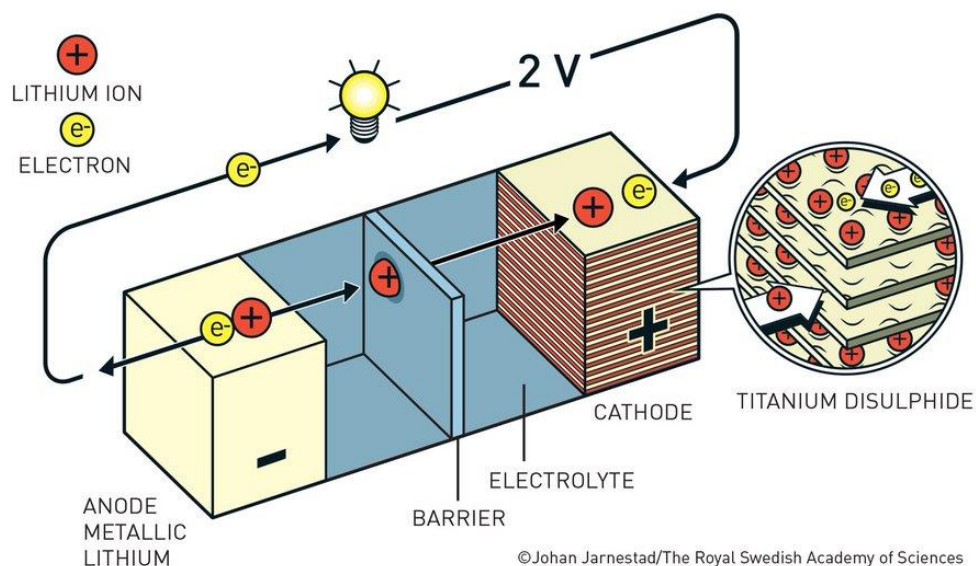


Figure 4. *Stanley Whittingham's battery configuration [27]*

This cell was put on hold due to several challenges including catching fire after short circuiting. John B. Goodenough, who is currently an engineering professor at the University of Texas at Austin, had the idea to change lithium cobalt with titanium disulfide. This paid off with a doubling of energy potential. It was not until Akira Yoshino of Meijo University in Nagoya, Japan made another swap that gave us the final piece that led us to the lithium-ion battery. Yoshino, by swapping pure lithium metal with petroleum coke doped with electrons, produced a safer battery whose safety was demonstrated by dropping iron balls on the battery [27]. With the research of these three, we got the discovery of the modern lithium-ion battery that we know today. Their efforts culminated in the 2019 Nobel Prize in Chemistry.

2.2 Zinc-Air Batteries

Zinc-Air batteries on the other hand, as a metal-air battery provide a much higher energy density. Current lithium-ion technology is still suffering from insufficient energy density, limited

to $<350 \text{ W h kg}^{-1}$ which has the inflated cost of $\$150\text{kW}^{-1}\text{h}^{-1}$. Zinc-air batteries however boast a large theoretical energy density (1353 W h kg^{-1} excluding oxygen) and a low cost ($<\$100\text{kW}^{-1} \text{ h}^{-1}$ and potentially $<10 \text{ kW}^{-1} \text{ h}^{-1}$) [13]. In the presence of O_2 , the Zn metal is known to oxidize to soluble zincate ($\text{Zn}(\text{OH})_4^{2-}$) ions [12]. First reported in 1840 by Smee, later showed the functionality with porous platinized carbon cathode in 1878, found commercial application in products on the market in 1932. The main appeal was the high energy density of $200\text{-}500 \text{ W h kg}^{-1}$ but unfortunately it boasts a poor power output. Research in the area though believes that Zn anodes with high active material utilization ($>80\%$), capability to deeply discharge and charge ($\text{DOD} > 50\%$) with reasonable cycle life (>500 cycles) and high coulombic efficiency ($>80\%$) should be achieved within the next ten years to make them commercially competitive [13].

2.3 Limitations in separator technology

In the development of battery cells, the separator is an area of concern as without the proper separator, the battery can short circuit and experience irreversible damage. Zn/Ni systems have been used to study Zn/ZnO systems due to the maturity of $\text{Ni}(\text{OH})_2/\text{NiOOH}$. In most Swagelok cells for the evaluation of batteries, woven separators dipped in electrolytes are often used in evaluating the electrochemistry of cells. However, non-woven separators have shown improved performance in these Ni/Zn systems and hinder dendritic growth of Zn [12]. Although some battery cells like liquid metal batteries are cheaper without solid separators, the lack of a solid separator causes the cell to be extremely hard to market for portable applications where a disturbance in the fluid layer could rupture the electrolyte layer. Electrolyte shorts between the positive and negative electrode could end up destroying the battery, even causing fires and explosions. Because of the ability to avoid not only reactant crossover but also completely circumvent metal dendrite concerns, solid separators are still relevant in battery cell research. In flexible applications for

rechargeable batteries, transferring aqueous electrolytes to shape-conformable solid-state electrolytes are essential. Porous separators are required to have a high absorption capacity and appropriate porosity to sustain electrolytes in their pores. In this area, the work of Kim et al. Prepared a separator with novel anionic exchanging coating on commercial propylene membranes. This ensured the membrane with an anion-repelling continuous phase due to the Donnan effect that disincentivized the transfer of zincates through the zinc air configuration [14]. Because most metal air batteries create oxidized metal reactants, avoiding the transfer of these can be a huge plus when optimizing metal air battery cells.

2.4 Liquid metal batteries

Liquid metal battery (LMB) research started based on grid storage. The idea was that the liquid anode, cathode, and electrolyte would give rise to superior kinetics and transport properties. Like most battery, LMBs allow for favorable chemical reactions to proceed in a controlled way by maintaining control of the battery with the right electrolyte. Keeping the electrodes separate if they are neutral but let them pass when ionized is the key to successful operation of the battery, especially without the presence of a solid separator. Below is figure 5 of a LMB configuration.

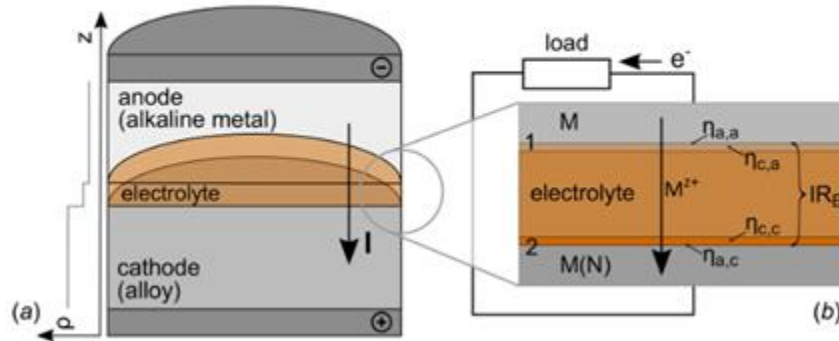


Figure 5. Liquid Metal Battery Configuration [15]

Since the negative electrode materials typically have a lower density than electrolyte materials, which have lower density than positive electrode materials, LMBs can be achieved on a density-based configuration. Most liquid metal cells are concentration cells and as such their open circuit voltage is solely given by the activity of the alkaline metal in the cathode alloy. These cells, however, eliminate the need for solid separators. However, LMBs are constrained according to the following, Liquid at practical temperatures (melting temp $<1000^{\circ}\text{C}$ and boiling point greater than 25°C), electrically conductive ($\sigma > 1 \text{ S cm}^{-1}$), and nonradioactive (I.e., available as a naturally occurring, stable isotope).

2.4.1 Aluminum Refinement Cells in the 1900s

To better understand the three-layer arrangement of liquid metal batteries we can investigate the three-layer aluminum refinement cell. This process was first proposed by Betts [16]. When later adapted by Hoopes, the goal of aluminum refinement was to manipulate the properties of metals and tendencies when dealing with electrolysis. Hoopes's design was based off the belief that when a current is applied in impure aluminum, the most readily oxidizable element present in the usual specimen of impure aluminum, the aluminum, will have a greater affinity for the cathode, rather than the anode that it came from. The anode in this case being fluorin (fluoride), ended up attracting the pure aluminum, creating this refinement process of pure aluminum [16]. Comparisons between these two starting configurations can be seen in figure 6.

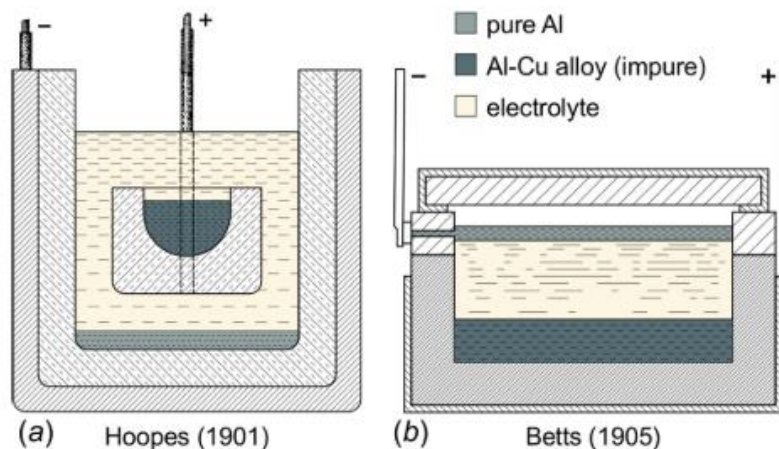


Figure 6. *Hoopes and Betts Liquid Metal Battery Configurations [16]*

Hoopes construction gives the division of the cell into two electrically insulated sections. Between them is a water-cooled section that is covered by a crust of frozen electrolyte providing electrical as well as thermal insulation. By arranging several graphite current collectors along the Al surface that provides a more evenly distributed current. In 1932 we saw super-purity aluminum become widely available with Gadeau's three-layer refinement process [24], that boasted a much lower operating temperature. Magnesite walls that could withstand the electrolyte attack without water cooling was a huge step forward. While the process of aluminum refinement has not seen much new research since, an understanding of the operation of these refinement cells can help us better understand the liquid metal battery.

2.4.2 LMBs with both metal cathode and anode

While lithium metal, with the high capacity of 3860 mAh g^{-1} and low redox potential of -3.04 when compared to standard hydrogen electrode, is considered as the optimal anode to boost energy density, the cycling performance during stripping-deposition is plagued by the dendritic growth, infinite volume change and continuous decomposition of the electrolyte [9]. liquid metal

anode adoption is a potential solution to the intrinsic dendrite problem of alkali metals. The theory behind this cell was the discharge products can be thermally decomposed at elevated temperatures to regenerate the original liquid metal reactants.

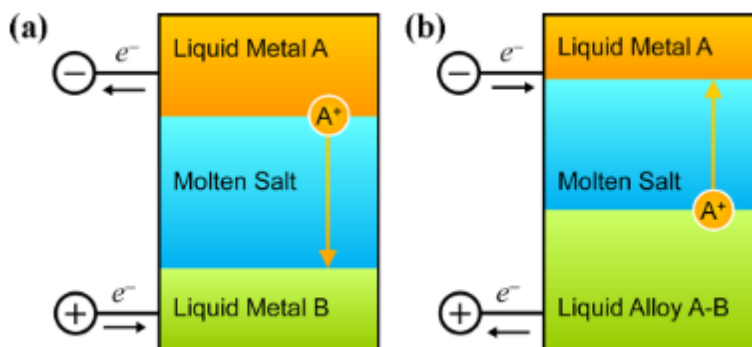


Figure 7. *Liquid Metal battery configuration with molten salt electrolyte [14]*

The first cell of this type was to follow the pattern highlighted in the figure 7 where schematic a show the battery upon discharging which (b) shows upon charging. For these two metal liquid battery configurations, we need to sort the two into groups of positive and negative electrodes. Electrode materials with a deposition potential more negative than $-2.0V$ are considered negative, while those more positive than $-1.0V$ are positive electrodes. Figure 8 shows the candidate metals separated by these positive and negative electrodes.

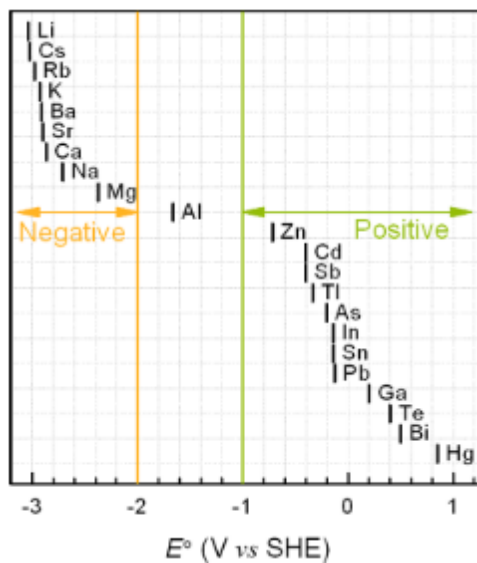


Figure 8. Deposition potentials of candidate metals [14]

As seen in the graph in figure 8, deposition potentials less than -2 constitute negative electrodes while those above -1 are considered positive. A strong interaction between the two is what provides the thermodynamic driving force we call the cell voltage. The battery cell like other cell configurations have the negative electrode layer give off electrons as it electrochemically oxidizes or loses its electrons. This metal will reduce in thickness as the cations or the metal ions without charge will travel through the molten electrolyte as they are conducted to the positive electrode. The positive electrode layer will inevitably grow in thickness as it forms a liquid A-B alloy. This process is reversible upon charging.

Alongside highly corrosive active cell components and high self-discharge rates due to metallic solubility of the electrode species, Liquid metal batteries lose their viability in not only bendable configurations but portable ones too. Moreover, three liquid layer configurations are overly sensitive to motion and in portable applications make them unreliable.

2.5 Gallium's reversible oxide formation

When considering gallium as a potential metal anode for a battery, the biggest advantage it has over other metals is its low melting point. Being able to exist as a liquid in near room temperature conditions, the option of a liquid metal air battery becomes a real-world possibility. In figure 8, from section 2.4.2, gallium has a higher E° than both lithium and zinc. For gallium to operate as the anode of the battery cell we need to consider a metal-air configuration rather than a two-metal liquid battery system. The transfer of the electrons in the gallium-gallic ion was first explored in the 1950s by William M. Saltman and Norman H. Nachtrieb. Their research focused on determining the standard electrode potential E^0 for this gallium-gallic couple. They found at around 25°C, the standard electrode potential was around -0.560 +/- 0.005 volts. This was close to the Von Bergkampff reported measurement of -0.52 volts.

In contrast to Na-K alloys that prefer to “give” the ions away from itself, Ga-based alloys prefer to “receive” ions from others [Next-Gen]. However, it is well known Ga_2O_3 shells form of a thickness of around 3nm [17] on the surface of gallium-based liquids when exposed to ambient air. This causes major problems where the movement of liquid metals in the device are required. Often though, to avoid contact between these surface-oxidized liquid metals and the microfluidic channel, liquids will work as a slip layer on the surface of the oxide shell. Other methods to reduce microfluidic channel include liquid metal marbles coated with iron (Fe) powder, PTFE powder, or graphene are proposed to reduce adhesion. In recent years other methods found include, suplyophobic surfaces as a method to reduce adhesion including engineered rough surfaces such as hierarchical micro/nanostructured surfaces, vertically aligned carbon nanotube surfaces and sand blasted aluminum have been reported as inherently nonwetting surfaces for liquid metal droplet manipulation [17]. Research done by Ziyu Chen and Jeong Bong Lee from the University

of Texas reported the use of gallium as a coating through evaporation to convert common microfluidic substrates to nonwetting surfaces against surface oxidized gallium-based liquid metal allows [17].

2.5.1 Phase Diagram of Gallium

As previously stated, gallium can alloy with other materials, which could potentially cause issues within the battery cell. Utilizing a phase diagram can help in determining if a substance will alloy with gallium. A phase diagram is a graphical representation of the physical states of substances under the effects of changing pressure and temperature. Typically, the diagram will have pressure on the vertical axis and temperature on the horizontal axis. Following the various lines and curves will indicate when a substance is subjected to a phase change. To show an example, figure 9 displays the phase diagram of gallium. It can be seen in the diagram that gallium at 300K, which is around 29°C, is in liquid form which is already known.

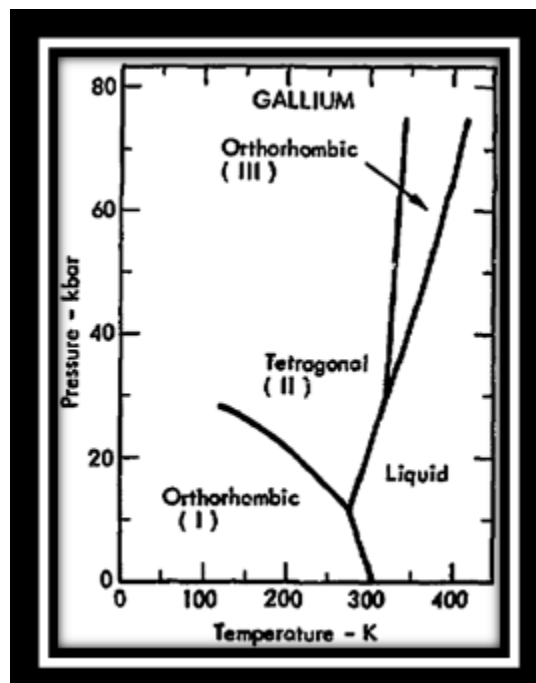


Figure 9. *Phase Diagram of Gallium with respect to Temperature and Pressure [21]*

Additionally, phase diagrams can also show the phase changes between two substances which can help to identify if they will alloy with one another. These diagrams will display temperature on the y-axis and atomic percent of the base substance, which in this case is gallium. This can be useful when trying to determine if the cathode material of the battery will alloy with the liquid metal anode. For example, a well-known cathode material used in liquid metal-air batteries is copper. figure 10 below is the phase diagram of copper and gallium which will show the tendency for these metals to alloy with one another. When choosing a material for the cathode, it is important that the anode and cathode do not alloy with each other because it could potentially cause issues such as shorting the battery.

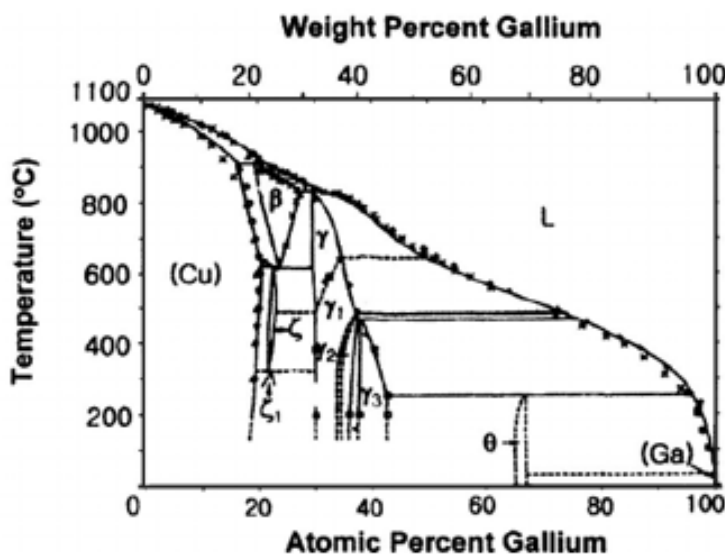


Figure 10. Phase Diagram of Gallium and Copper [22]

Looking at this diagram, Cu and Ga will alloy at low temperatures, which means it may not be the best choice for the cathode material. Although copper does function as a cathode, the low alloying temperature may cause issues with gallium since Ga has a low melting point. Ensuring the cathode material will not alloy with the gallium anode would avoid issues like shorting the battery, but additional research must be done to find the appropriate material.

2.5.2 Materials that Will not Alloy with Gallium.

As previously, it is important that the anode material, in this case gallium, will not alloy with the electrode material. This means that the electrode must be a material which will not tend to alloy with gallium at lower temperatures. Copper, as seen in the diagram in figure 10, is a softer and less durable metal, so it makes sense that Cu may not be the best option for an electrode. A stronger and more durable metal will allow for maximum mass electron transfer and have a less likely chance of alloying. Stronger materials which could potentially work as an electrode material with gallium include platinum (Pt), gold (Au), silver (Ag), and tungsten (W). To show an example of this, figure 11 is the phase diagram of gallium and tungsten. In the diagram

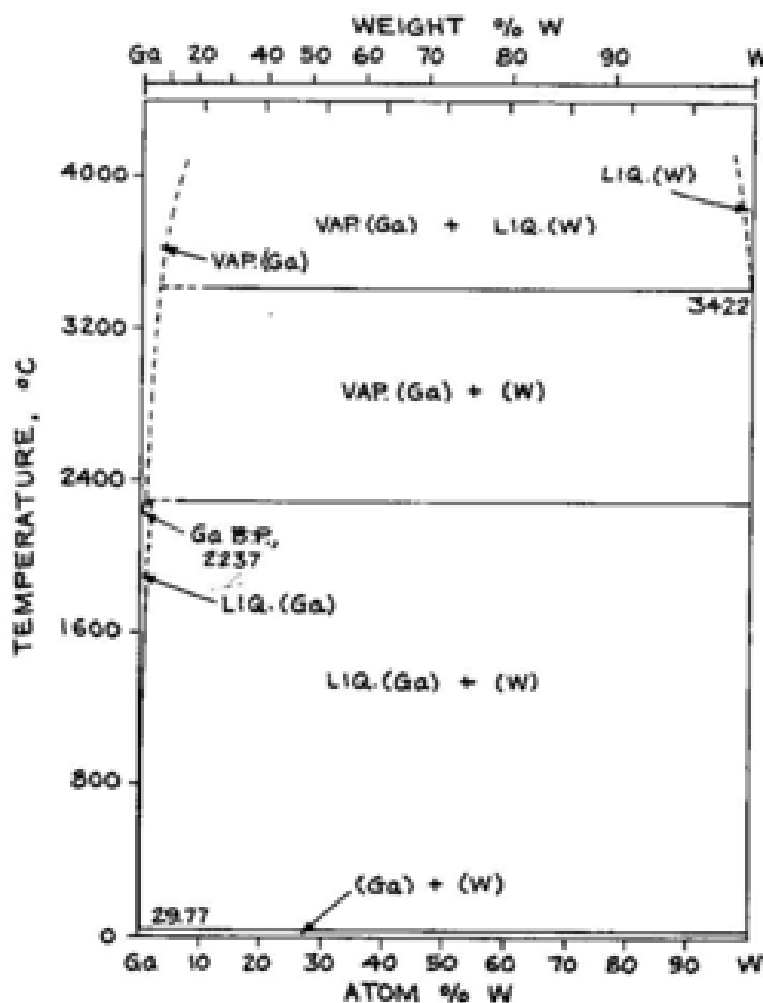


Figure 11. Phase diagram of Gallium and Tungsten showing a much more favorable electrode than copper shown in Figure 10 [23]

both Ga and W are displayed with their various phases at different temperatures. According to this diagram, as temperature increases, gallium and tungsten will remain in distinct phases which means they will remain separate. This is an ideal quality for an electrode material because this material will not alloy with gallium even at different temperatures. Phase diagrams can be useful when determining materials tendencies to alloy with one another, however additional testing and experimentation is needed to make conclusions.

2.6 Previous Relevant Work

This work originated from the 2015 MQP “A New Liquid Metal-Air Battery” which investigated the concept of a liquid gallium-air battery and was further developed in 2016 with *Liquid Metal-Air Battery for Energy Storage* [20], 2017, with *Investigation of the Rechargeability of a Liquid Metal-Air Battery* [35] and 2020 with *Feasibility of Ambient Temperature Liquid Metal Air Batteries* [36] at WPI. These MQPs were able to confirm that a gallium-air battery type was possible and could potentially surpass the capabilities of commercialized metal-air batteries. The battery configurations created by these groups were successful in discharging the test cells but ran into issues when trying to recharge the cells. However, the 2020 test configuration was able to show the ability to recharging. Gallium shorting and poor contact areas were obstacles which made the configurations unlikely to work as a flow battery. Additionally, more research and testing need to be done to find an enhanced electrolyte, which has shown to improve Ga redox reversibility. Oxygen is an important aspect to this battery cell and needs more investigation into the effects of its dependence and limiting factors in the absence of it. Although liquid metal air batteries may not be economically feasible, understanding their performance is important to expand the potential of high energy density batteries.

2.6.1 Work Achieved by 2015 MQP

This MQP work first started in 2015 by Tyler Howard, Laura Merrill, and Stephen Johnston who sought out to create a liquid metal air battery. This team was able to establish a proof-of-concept liquid gallium air battery which was further developed in the following years. The concept of this battery was tested using a prototype Swagelok test cell design through a flat constant discharge which was able to determine the limiting factors of their set up. The goal of testing this cell design was to investigate the feasibility of a Ga-air electrochemical cell without needing a flow system. However, this test cell design lacked the dynamics of a flow configuration, so modifications to the cell needed to be investigated. Various tests were run to investigate several aspects of this battery concept.

Their first test consisted of analyzing the discharge and polarization performance at various temperatures which were compared to theoretical values as well as values of commercialized Zn-air batteries. The battery cell consisted of a pure Ga anode, a 6M potassium hydroxide (KOH) aqueous electrolyte which was soaked in a Zirconia (Zr) cloth separator, and to improve O₂ reaction kinetics a platinum-catalyzed gas diffusion layer (GDL) was added. The test cell had a flat discharge time of 10 hrs. with a constant current drain at 50-60°C and an open circuit voltage of 1.1-1.4V for the initial test. The results showed that the capacity of the test cell was much lower than that of a commercialized Zn-air battery cell. The hypothesized limiting factors of the battery cell which may have caused the decreased capacity included separator drying, formation of an oxide layer, and electrolyte carbonation. Additionally, theoretical analysis of gallium reactions was done to verify the unknown resulting product of the reaction.

After numerous testing with different configurations and components, this group was able to make a few conclusions. One main hypothesis the group made was the limiting factor of carbonation at lower potentials may have caused the Ga cell to only make small contact with the electrolyte. This is different from Zn-air battery which outperformed this prototype due to Zn powder directly being mixed into the electrolyte, which allowed for direct contact. Furthermore, a Zr cloth was found to be the preferable anode separator and electrolyte interface material. However, the separator was gallium absorbent, which resulted in wetting Ga into the cathode material which shorted the battery. Additional research needed to be done to overcome these issues.

2.6.2 Work Achieved by 2016 MQP

In the following year, Victor Hu, Huyen Vu, and Jacob Zargorski continued the work by testing different electrolyte layers as well as addressing the potential rechargeability. These tests were attempting to reduce the limiting factors outlined in the previous work, which were the impacts of electrolyte drying and carbonization. To optimize the battery, alterations to the cell were made including testing with alumina cloth, gelled PVA/KOH, increasing the KOH concentration, and two KOH soaked Zr cloth separators. Test results found that utilizing two Zr cloth separators demonstrated an improved performance, having doubled the discharge duration. This indicated that carbonization may be the key aspect which limits discharge durations and performance. [20]. Additionally, these Zr clothes went through the resoaking process, which revealed the hydroxide was a critical limiting factor of the reaction. Additional experiments were run to test different concentrations of the alkaline solution to make improvements to the electrolyte layer. Both 6M and 8M KOH were tested, and the 6M concentrations provided improved performance. Further testing was done which investigated the optimal temperature to run the

system at. This was done between 40-70°C at 5-10° intervals, and peak performance was found to run at 50°C.

After the results of the experiments and testing, the team gave a series of recommendations which could further improve the state of the liquid Ga-air battery. The first suggestion was to create a new configuration which is like that of a flow battery where liquid gallium and the electrolyte are continuously circulated throughout the process. Applying this type of configuration could potentially allow for larger discharge durations. This is because the film formation of gallium-oxide between the layers and the buildup of potassium carbonate in the separator could be prevented. The diagram in figure 12 displays a potential schematic for this battery configuration.

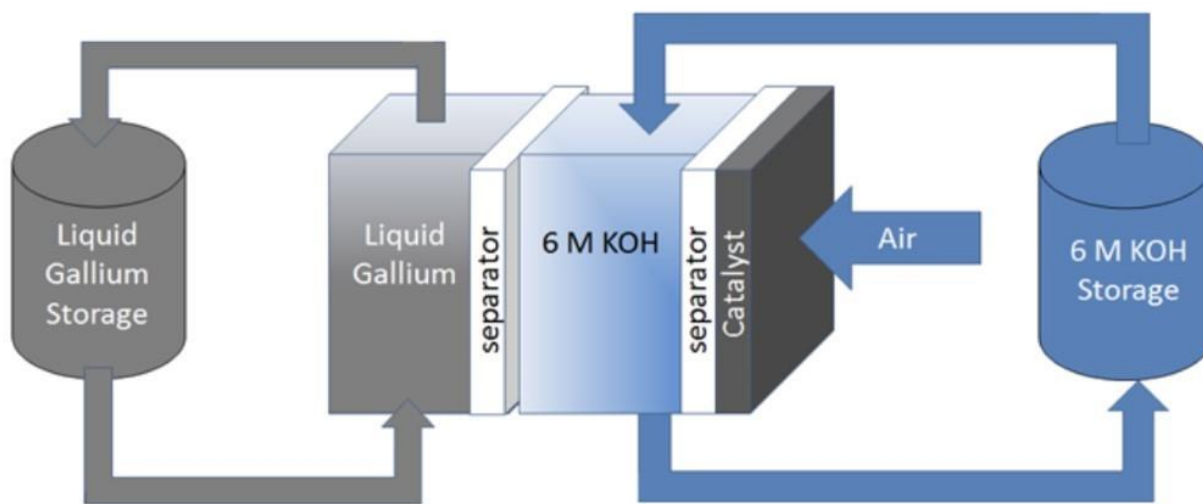


Figure 12. Potential Gallium-air battery flow configuration [20]

Further investigation of a commercialized MnO_2 gas diffusion layer is necessary due to it being an inexpensive alternative to a platinum-based catalyst. Additionally, manganese oxide has recharging potentials which would make grid-scale energy storage possible. Applying ionic liquids could also make improvements to this battery configuration due to the lack of water content which avoids evaporation and could extend the discharge durations and overall performance. Finally,

additional research into gallium itself is necessary in understanding its electrochemical properties and interactions with the different layers. A series of characterization techniques, such as XRD or SEM, would help to understand the primary gallium reaction taking place within the cell.

2.6.3 Work Achieved by 2017 MQP

The 2017 MQP group, Allison Marx, and Kelly Rapoza, carried out additional testing on a Swagelok prototype cell to continue the previous work of this project. Overall, this project was able to achieve success in improving the discharge time and rechargeability through investigating different metal anode and electrolyte options. However, before they could do this, the specific chemical reaction of gallium within the cell needed to be determined. There were two viable compounds which could be produced, gallium hydroxide and gallium oxide. Tables 1 and 2 are tables which outline the possible reactions taking place.

Table 1. Open Circuit Voltage for Gallium Hydroxide Product [34]

Electrode	Reaction	Potential (V)	ΔG^0 (kJ/mol)
Anode	$\text{Ga} + 4\text{OH}^- \rightleftharpoons \text{Ga}(\text{OH})_4^- + 3\text{e}^-$		
Anode	$\text{Ga}(\text{OH})_4^- \rightleftharpoons \text{Ga}(\text{OH})_3 + \text{OH}^-$		
Overall Anode	$\text{Ga} + 3\text{OH}^- \rightleftharpoons \text{Ga}(\text{OH})_3 + 3\text{e}^-$	$V_A^0 = -1.242$	-360
Cathode	$\text{O}_2 + 2\text{H}_2\text{O} + 4\text{e}^- \rightleftharpoons 4\text{OH}^-$	$V_C^0 = +0.401$	-155
Overall	$\text{Ga} + \frac{3}{4}\text{O}_2 + \frac{3}{2}\text{H}_2\text{O} \rightleftharpoons \text{Ga}(\text{OH})_3$	$V^0 = V_C^0 - V_A^0$ $V^0 = 1.643 \text{ V}$	-476

Table 2. *Open Circuit for Gallium Oxide Product [34]*

Electrode	Reaction	Potential	ΔG^0 (kJ/mol)
Anode	$\text{Ga} + 4\text{OH}^- \rightleftharpoons \text{Ga}(\text{OH})_4^- + 3\text{e}^-$		
Anode	$\text{Ga}(\text{OH})_4^- \rightleftharpoons \text{Ga}(\text{OH})_3 + \text{OH}^-$		
Anode	$\text{Ga}(\text{OH})_3 \rightleftharpoons \text{Ga}_2\text{O}_3 + 3\text{H}_2\text{O}$		
Overall Anode	$\text{Ga} + 3\text{OH}^- \rightleftharpoons \frac{1}{2}\text{Ga}_2\text{O}_3 + \frac{3}{2}\text{H}_2\text{O} + 3\text{e}^-$	$V_A^0 = -1.323$	-383
Cathode	$\text{O}_2 + 2\text{H}_2\text{O} + 4\text{e}^- \rightleftharpoons 4\text{OH}^-$	$V_C^0 = +0.401$	-155
Overall	$\text{Ga} + \frac{3}{4}\text{O}_2 \rightleftharpoons \frac{1}{2}\text{Ga}_2\text{O}_3$	$V^0 = V_C^0 - V_A^0$ $V^0 = 1.724 \text{ V}$	-499

Using X-ray diffraction, the group was able to identify the reaction within in the battery with a 6M KOH electrolyte was forming gallium oxide. Additionally, a gallium tin alloy, 92% Ga 8% Sn, was proven to be a viable option for the anode material. Utilizing the alloy lowered the cost of the battery, and at optimal conditions of 60°C with 6M KOH and 0.17M gallium oxide electrolyte mixture proved to result in longer and more stable discharge runs over pure gallium. Electrolyte evaporation and electrolysis of water prevented the battery from charging due the presence of water in the electrolyte. Their tests proved that tetrabutylammonium hydroxide ionic liquid is a feasible electrolyte for a gallium-air battery. Rechargeability of the battery was possible with a 20-minute discharge after recharging.

Like past projects, this group also recommended that this battery should be adapted into a flow battery configuration [34]. This would allow for more energy to be stored due to its ability to decouple energy and power within the battery. Applying liquid gallium through this configuration would allow gallium oxide formation to be minimized as well as increasing the discharge time.

Ideally, tetrabutylammonium hydroxide ionic liquid electrolyte should function well with pure gallium. Once this is confirmed, more testing needs to be done to make concrete conclusions on ionic liquid and gallium-tin alloy. Moving forward, additional improvements need to be made for the electrolyte separator. This group used a Zr woven cloth type ZYK-15 with a coarse weave and large pore size which is soaked in the desired electrolyte which functions well for aqueous electrolytes. However, the main issue was the separator experiencing leakage of gallium into the cathode which short circuited the battery. The investigation of a new separator with an ionic liquid would address the leakage issue. The potential use of a polymer electrolyte membrane may provide the needed barrier while maintaining ion exchangeability.

2.6.4 Work Achieved by 2020 MQP (Latest)

The latest group to continue this work was in 2020 by Ari Athair and Tristan Arnold, who also utilized a Swagelok test cell to make further improvements to the liquid gallium-air battery configuration. This group looked at the fundamental reactions in the test cells through Cyclic Voltammetry (CV) testing to determine its reversibility potential. The CV test proved especially useful in determining the reversibility of a reaction and can study the reduction and oxidation process of molecular species by applying a voltage difference in a pyramid wave form and measures the resulting current. figure 13 shows the ideal shape a voltammogram will have if a reaction proves to be reversible. This is known as the “duck” shape.

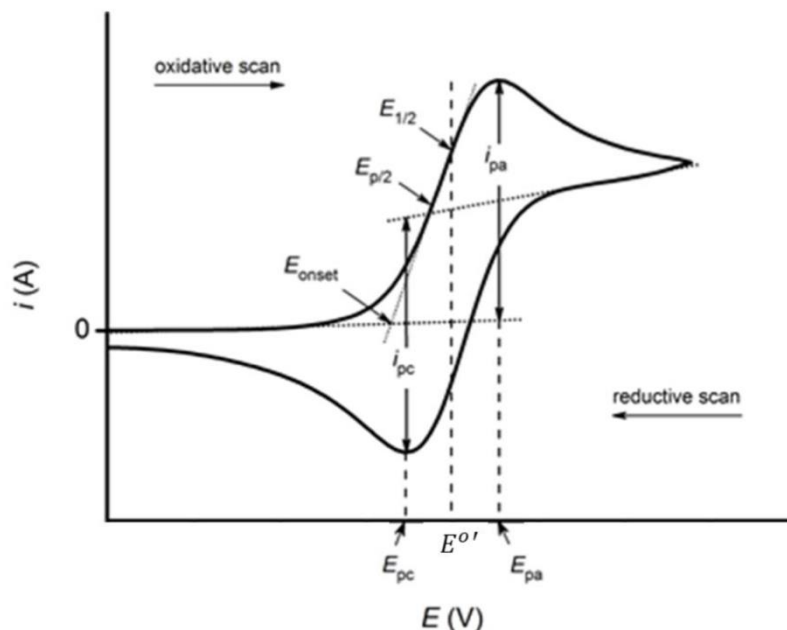


Figure 13. “Duck” shape voltammogram curve which indicated reversibility [35]

The reaction of gallium to dissolved gallium oxide reactions showed the ability to be reversible through CV test analysis. Reversibility and stability were further increased when a 0.1M dissolved Ga_2O_3 was added to a 6M KOH electrolyte. This groups Zr cloth separators also experienced gallium seepage and shorting of the battery, so a polypropylene separator was added to the prototype test cell. This addition made the first charge discharge cycle a success. Furthermore, polarization curves of the new test configuration were compared and showed higher discharging voltage and stability than that of a commercialized Zn-air battery, although more testing on needs to be done. The test cell also proved to run better than a Zn-air battery at high current densities as well as maintaining its potential at these densities, which indicated faster reactions and transport of liquid gallium. Additionally, the voltage at low currents of a discharging Ga battery was able to near its open circuit voltage. Limitations including electrolyte drying, battery shorting, and electrolysis all attributed to the short discharge lengths of the battery.

Although this group was able to produce strong results which prove the concept of a liquid gallium-air battery, there was still additional research and experimentation to be done. Applying a flow battery configuration seemed to be less likely due to Ga seepage and poor contact areas. Additional CV testing was also thought to help the future of this work. The CV tests not only would benefit the understanding of the internal chemistry, but also could be used to determine the internal diffusion coefficient of different configurations. Furthermore, this group made a few recommendations which could improve the overall performance and potential of a liquid Ga-air battery. First, an electrolyte additive has shown to improve Ga redox reversibility but needs more researching and testing to make an appropriate choice. An investigation needs to be done to determine the systems oxygen dependence and in the case of its absence. Changes to Swagelok components could decrease internal resistance which could improve voltage readings and lead to further innovations of a liquid gallium-air battery.

2.6.5 Gallium and its redox reaction powered self-actuation

A previous experiment conducted by Ryan Gough and others at the University of Hawaii titled “Self-Actuation of Liquid Metal via Redox Reaction” is a significant component in this gallium-based battery project. In the Gough paper, a technique was described to cause a gallium-based alloy to actuate without the requirement of an external power supply. This occurrence is made possible through the cell’s construction. The cell in the Gough experiment contains anodic and cathodic reservoirs, each with a height of 400 μm and a diameter of 10mm. The parts of “anodic reservoir” and “cathodic reservoir” are used as placeholders to denote sections where the electrons are produced and received in. The configuration illustrated in this paper is not a battery and as such it cannot be labeled accordingly, despite the experimentation being carried out to determine the viability of a gallium-based metal air battery. In the bottom of each reservoir, there

sits a copper electrode. Between the reservoirs is a capillary channel filled with 0.25 NaOH solution. The cathodic reservoir is exposed to oxygen and the anodic reservoir, containing a flake of aluminum and the Galinstan; a gallium based liquid metal alloy, is covered to prevent oxygen from entering.

The cell described by the paper acts as a self-propelled motor due to its energy derived by a redox reaction between the Galinstan and a flake of aluminum. When Galinstan and the aluminum make contact as they are submerged in the electrolyte, it forms a galvanic cell. A galvanic cell is an electrochemical cell in which spontaneous redox reactions produce electrical energy [30] that results in a surface tension gradient along the length of the liquid metal [19]. Inside this galvanic cell, gallium is assumed to eat away the oxide layer that forms on aluminum, exposing it. aluminum will begin to react rapidly with water to form hydrogen and aluminum oxide. This concept has developed by a Purdue University engineer for the purposes of developing hydrogen air [31].

To achieve the actuation using minimal voltage and power, a technique known as electrowetting is used. Electrowetting on dielectric (EWOD) is a technique that removes the need for a pump to achieve a modest deformation of liquid metals. When the cell's electrodes are not exposed to a voltage, the surface of the electrode exhibits and provides hydrophobicity i.e., it repels water. However, when the cell's electrodes are exposed to a voltage from an external electrical connection, the electrode's surface will form a temporary hydrophilic surface i.e., it is capable of being wetted. When the surface of the electrode is hydrophilic, it induces the aqueous Galinstan to wet the surface of the electrode. Once the surface is wetted, the cell initiates galvanic actuation. Actuation is the act of propelling something and in this case, the Galinstan is propelled via Laplace pressure from the anodic reservoir and into the capillary channel. The Galinstan returns quickly to

its reservoir once the electrical connection is broken. Once this connection is broken, the redox reaction that was fueling the actuation is ended. Because gallium based liquid metal alloys produce an oxidation layer of Ga_2O_3 that forms rapidly, and it sticks to every surface [18] including the capillary channel. The oxide coating the capillary channel is dissolved by the NaOH solution which forces the Galinstan back into the anodic reservoir. This entire process can be repeated and is also reversible. This process is shown below in figure 14.

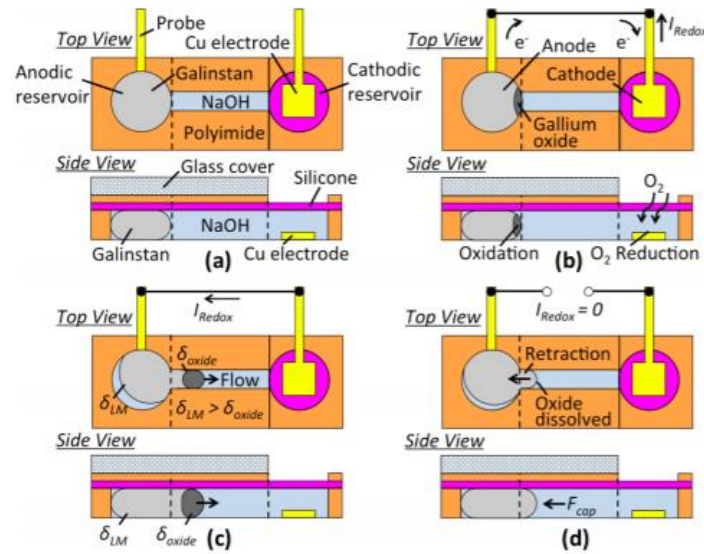


Figure 14. The process of Galvanic actuation between the two reservoirs [19]

The Gough configuration illustrated how the formation of Ga_2O_3 occurs but with its formation comes unavoidable problems as well as some advantages. When the gallium is exposed to air, Ga_2O_3 is formed on the exterior of the liquid metal. Gallium oxide's main problems are that it interferes with the wetting behavior and obstructs both electrical and physical contacts. This can lead to the cell to experience issues with short circuiting. Some advantages brought forth by the formation of gallium oxide include that its presence helps stabilize the liquid mechanically and decreases the interfacial tension between the electrolyte and liquid metal [19]. The combination of the oxidizing reaction with the sodium oxide in the channel creates a thinner layer of hydrophilic

gallium oxide without mechanical obstruction that would come with a thicker layer of gallium oxide [19].

While the configuration described in detail from the Gough Paper was not inherently a battery, it displayed aspects of a battery which could be applied to a battery configuration. For example, just like all other batteries, the cell was able to create and sustain a current from its redox reaction. The Gough configuration was unique in how it self-actuates and can cycle the gallium so that fresh gallium is exposed to the cathode. This configuration was also able to alleviate some of the issues that coincide with the buildup of gallium oxide that often results in the cell short circuiting. This was made possible because the sodium hydroxide electrolyte dissolved the hydrophilic gallium oxide.

2.6.6 “Soft, Highly Elastic, and Discharge-Current-Controllable Eutectic Gallium Indium Liquid Metal-Air Battery”

In 2018, gallium was included in a eutectic gallium-indium liquid metal (EGILM) in the Majidi lab to prepare a stretchable, high-k dielectric elastomer [29]. Eutectic for reference is when a mixture of substances that melt and solidifies at a single temperature that is lower than the melting point of the separate constituents. This is extremely important for metal batteries where we want to have the liquid metal properties of gallium at room temperature. EGILM is sufficiently stable in air and water environments without firing. The configuration of the cell was based on an EGILM anode with an elastic poly (acrylic acid) (PAA)-based gel electrolyte film, and a carbon fiber yarn coated by a Pt nanoflower array as the cathode. This was presented as a cable-shaped, soft, highly, elastic, discharge-current-controllable liquid metal-air battery with high discharge performance. Figure 15 below shows the methodology of manufacturing the battery and what character traits the unique configuration provides.

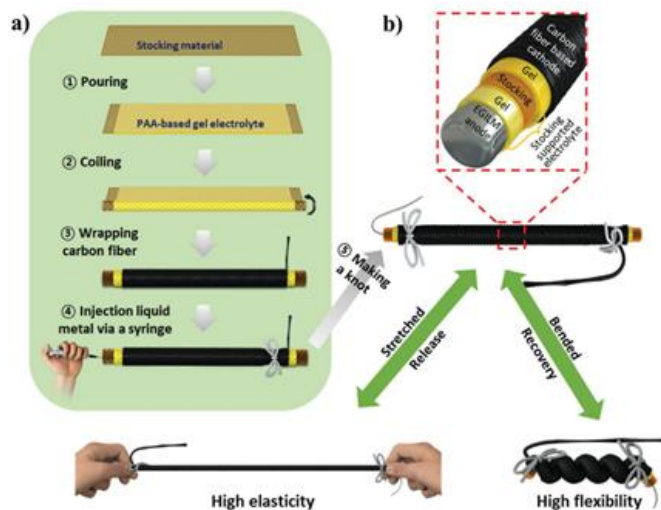


Figure 15. Cable-shaped eutectic gallium-indium liquid metal-air battery. A) highlights the methodology for creating the battery and b) shows the components and characteristics of elasticity and flexibility [29]

The module was built with nylon stocking material immersed in a mixed solution consisting of a PAA based polymer precursor solution and a polymerization initiator to realize a stocking –supported gel electrolyte films. This was made to enhance the mechanical strength of the gel electrolyte film to carry the EGILM and preserve the shape of the battery. A carbon fiber-based cathode is wrapped around the surface of the cannular cavity. Last step was to inject the EGILM inside the cannular cavity. The tensile properties of the battery allowed for feasible adjustments to a diameter of 10 μm , implying the shape can go from cable like to fiber like. The prototype battery in the paper was a length of 12 cm (about the length of the long edge of a credit card) and a diameter of 8mm.

Tests for corrosive resistance were done for EGILM, gallium, indium, aluminum, and zinc were done by immersing them in 37.5 wt% KOH aqueous solution. Aluminum was the fastest, zinc and gallium had similar gas production rates while indium showed almost no bubbles. EGILM showed better corrosion rates than gallium due to indium inclusion. 3 cable-shaped metal-air batteries were tested, gallium-, EGILM-, and indium-air batteries. The discharge performance of

the indium-air battery was negligible due to low electrochemical activity and high hydrogen evolution overpotential of indium. This test shows that the EGILM-air battery derives its discharge performance solely from gallium. For improving the oxygen reduction rate of the cathode, classical Pt catalyst was coated on the surface of the carbon fibers by a pulse electrodeposition method. The positive results of this are shown in figure 16.

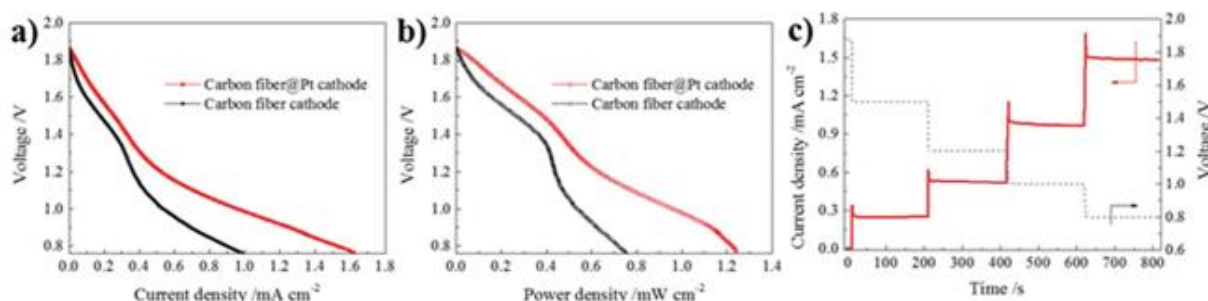


Figure 16. Oxygen reduction rate improvement from Pt catalyst coating [29]

This battery configuration was tested through an open-ended battery configuration with EGILM as the anode and carbon fiber yarn as the cathode in a 37.5 wt. % KOH solution in the glass beaker as seen below in figure 17.

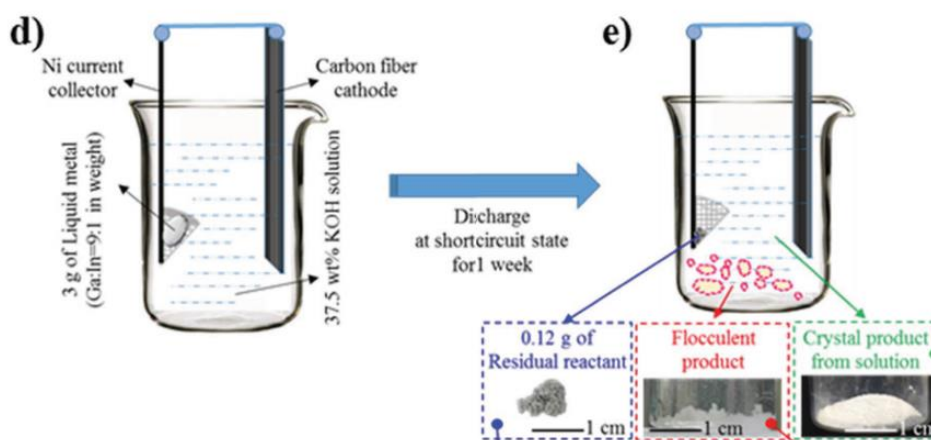


Figure 17. Open-ended battery configuration of the EGILM and carbon fiber yarn cell [29]

After 3 weeks of discharging reactions under short-circuit conditions showed 3 products are produced. Residual reactant in the anode (Indium), Flocculent product on the bottom of the beaker ($\text{In}(\text{OH})_3$), and the crystal product obtained by neutralizing the alkaline electrolyte with HCl and crystallization form the solution (GaOOH). These results point to a part of indium and all of gallium in the EGILM participating in the discharge reaction to generate trivalent products. The remainder of indium solidified into an indium metal block.

Table 3. Reactions of the EGILM-air battery [29]

<i>In the Anode</i>		<i>In the Cathode</i>	
$\text{Ga} - 3e^- \rightarrow \text{Ga}^{3+}$	(1)	$2\text{Ga} + 6\text{H}_2\text{O} - 6e^- \rightarrow 2\text{Ga}^{3+} + 3\text{H}_2$	(4)
$\text{In} - 3e^- + 3\text{OH}^- \rightarrow \text{In}(\text{OH})_3$	^[54,62,63] (2)		
$\text{Ga} + \text{In}^{3+} \rightarrow \text{Ga}^{3+} + \text{In}$	^[54,62] (3)		

Indium is the inhibiting factor for gallium corrosion due to its high hydrogen evolution over-potential. Before forming $\text{In}(\text{OH})_3$, the indium in EGILM first changes to In^{3+} ions as seen in equation 3 of Table 3. PAA-based gel electrolyte film with 1mm thickness exhibits good elasticity and strong adhesive ability. EGILM-air battery exhibits the highest power density (0.265 mW cm^{-2}) at 1.5V. They also found that the configuration was pressure dependent where the current would rapidly recover when pressure was released. For wearable electronics, current fluctuation on slight pressure is disadvantageous. In the future, supporting substrate buried in the gel electrolyte film can be changed from the soft stocking material to more rigid material with porosity and flexibility. It is important to note that a 25% stretch increased the discharge current from 16.768 to 16.919 mA. The increased contact area between the anode and electrolyte. The Discharge rate did not decrease whether stretched 60% or 100%. Figure 18 shows the effects on the discharge current of the cable-type battery.

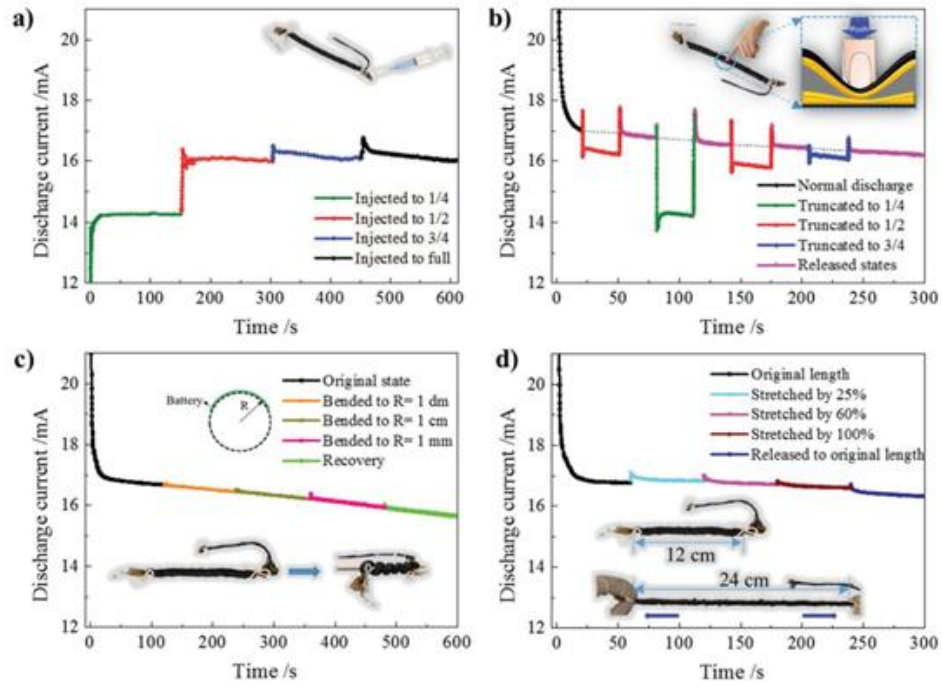


Figure 18. Effects on the discharge current of the cable-cell a) highlights the effect of injection % b) highlights the effect of truncation c) highlights the effects of twisting and d) highlights the effects of stretching [29]

3. Methodology

The goal of our project was to further the work of prior MQPs by adding increased visibility and flexibility. The creation of this type of battery would be a major advancement for battery development. To achieve this goal, we made our objectives as follows:

1. To develop a 2-Dimensional electrochemical cell for observing gallium oxidation.
2. Effectively construct and troubleshoot the battery cell module with increased visibility, matching observed physical phase behavior to electrochemical measurements.
3. Demonstrate battery discharge in a flexible form factor.

By introducing the aspect of increased visibility for testing and experimental purposes, we hope to solve the issues of the previous MQPs not being able to get visual cues as to what chemical reactions happen inside of the cell. A trait that could help propel optimization of this cell type in the future. Flexibility is a secondary factor we wanted to introduce to open the up the entry point into the market for metal air battery cells. Flexible metal-air battery applications can help to solve the issues some wearable electronics are experiencing in terms of cell size and rigidity in their energy storage cells. The following sections will outline the building of both the experimental cells and the experiments we carried out.

3.1 Baseline performance with the Gough Configuration

The design of the configuration used in the lab was a recreation of the Gough experiments. Since the gouge configuration showed a one-time use configuration with the inclusion of aluminum, we started our first round of tests absent of aluminum. With the same Battery analyzer used by previous MQP groups, we aimed to see how viable the charge and discharge cycles were for the Gough configuration. The goals behind this decision were to check a few things.

1. How important is the isolation of gallium and other soft metals inside Galinstan into their base form and if this increase is what helps to really propel the surface tension difference.
(This could be seen in increased speeds at comparable currents)
2. Can the module be considered rechargeable? (Do charge and discharge cycles give diminishing returns on subsequent cycles)
3. How much charge does the module hold on charge and how long is the discharge cycle?
Does the length of the channel cut the charge/discharge cycle potential short?

With these 3 aims in our sights for our first round of tests, we hope to meld the visibility of the module proposed in the Gough paper with the chemistry in previous gallium air MQPs. Figure 19 shows a simple diagram of the Gough configuration used to run these tests.

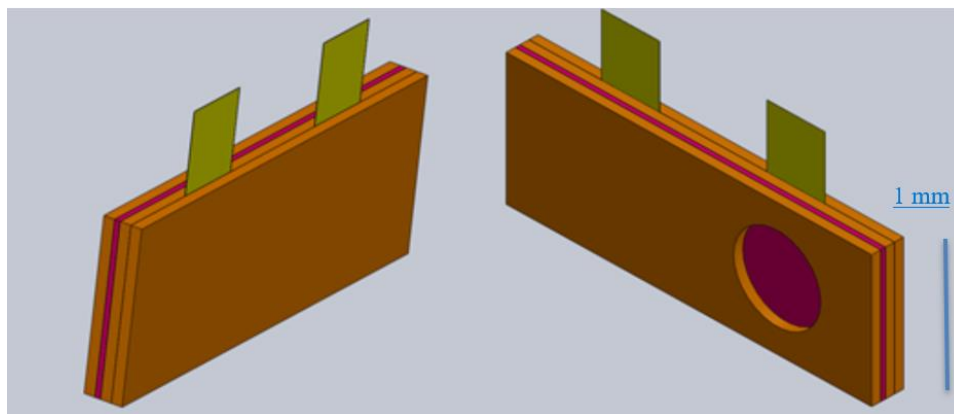


Figure 19. *Gough Configuration Design made in Solidworks*

3.2 Materials

When deciding on our materials for our first rounds of tests, we wanted to choose materials that merge the types and functionality of both the Gough paper's configuration and previous MQPs. This would allow us to easily scale up our initial tests from more of the gouge configuration to a final metal-air battery configuration. Additionally, each component needed to be bendable to create the desired flexible battery cell design. The structure of the cell was made of thin layers

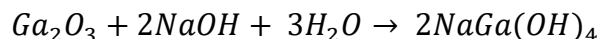
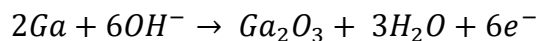
stacked on top of one another to make for easy assembly. This was made from a roll of polyimide tape we could cut up off the roll and peel layers to fit the thickness we wanted to best match the Gough configuration. Electrical grade Kapton polyimide tape from Tapes Master was used for the polyimide layer with a film thickness of 1.2 millimeters and was specifically chosen due to its transparent properties on top of its low cost. Transparency allowed for a clear view of what was going on in the cell which helped to better understand the overall electrochemistry. For the silicon layer a rubber sheet, elevated temperature, transparent and heat resistant 0.5mm silicon was used from the brand Laimeisi. The cathodic reservoir was only covered by the sheet of silicon which allowed for it to be oxygenated. Additionally, a conductive copper foil electrical tape purchased from McMaster-Carr was used for the electrode probe and has a width of ¼ in. This layer provided current throughout the cell, and the adhesive layer is nonconductive so it would not interfere with the experiments. Finally, a low melting point alloy Galinstan was purchased from RotoMetals, which is composed of 68.5% Ga, 21.5% In, and 10% Sn. The Galinstan is put into the anodic reservoir, while 37.5 wt.% KOH is inserted throughout the channel and both reservoirs. All materials purchased for the duration of the project can be found in a table in Appendix E.

3.2.1 Material Differences

To better understand the concepts behind the Gough paper, we started with recreating their experiment. This required using the same materials to build the configuration as well as applying similar methods as their experiments used. The paper proposes a two-circular reservoir (400 μm deep and 10 mm diameter) module with a 2mm wide channel that runs between them. One side holds a droplet of Galinstan that takes up the volume of the reservoir with a flake of aluminum foil while the channel and the other reservoir holding 0.25M NaOH electrolyte. Our module's reservoirs were punched out by a 3/8th inch hole punch which equates to around 9.525 mm. the

channels were reproduced perfectly, however. This only resulted in a volumetric change of less than 3 mm². It is important to note we chose instead to use 37.5 wt.% KOH instead of 0.25M NaOH. This choice was done as our second supporting source had a successful flexible gallium air configuration. This is a huge change to consider as 37.5 wt. % KOH is around 9.1M KOH compared to 0.25M NaOH. This means that while both are way off the pH scale (both are pH > 35), the difference is 1.56 in favor of the 37.5 wt. % KOH.

The exclusion of NaOH from the module also removes the potential formation reaction of gallium oxide with sodium hydroxide molecules. While the OH^- ion contributes to the formation of gallium oxide, water and electrons, sodium hydroxide molecules can also contribute to further dissolving the gallium oxide layer that forms on the surface of the Galinstan droplet. Both equations are as seen below.



We can assume the KOH would function We can assume the KOH would function like the sodium hydroxide as both electrolytes create an environment with a high enough pH to allow the formation of gallium oxide and the dissolving of gallium oxide.

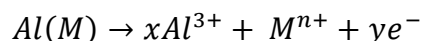


Figure 20. Galinstan droplet preparation inside of a Self-Actuation test module

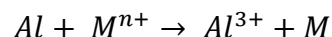
Both reservoirs have copper strips on the bottom that when closed allow for an easy transfer of current between the reservoirs. Copper strips were eventually cut thinner to avoid leaking through copper strips during experimentation.

3.2.2 Aluminum Inclusion

The reason they include an aluminum flake inside of the cell is because Galinstan (more specifically gallium) is known to strip the oxide layer on aluminum that often protects it from its very spontaneous reaction with water. This phenomenon is known as the Rehbinder effect. The reaction between gallium and aluminum is as follows:



The gallium and aluminum will react together to make this metal allow seen as Al(M) where M is our low melting point metal. As the reaction happens, the aluminum becomes exposed in its Al^{3+} form while gallium breaks off in its base form. The important part of this equation is the release of electrons. The following electrochemical exchange reaction occurs between the cathode ions (M^{n+}) and the Al.



If the two copper strips are connected, the open reservoir in the configuration will act as a cathodic area, allowing for the release of electrons from the now anodic reservoir with aluminum and gallium to the open cathodic area as demonstrated in the equation above. The gouge paper recorded the current of this electron flow vs. speed of the Galinstan head to demonstrate the relationship between the rate of the internal reaction forming base gallium (M) vs. the speed through the channel as seen in figure 21.

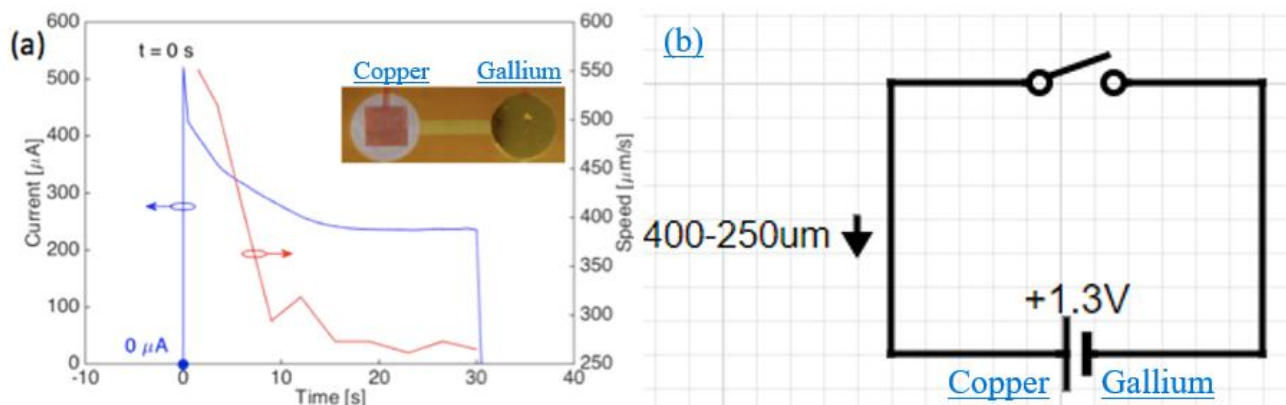


Figure 21. Left Current and Speed Results from Gough Experiments. Right Circuit diagram showing flow of current in relation to the image of the system in the graph to the left.[19]

The first peak indicates the point at which or slightly after the aluminum flake was added to the anodic reservoir and the reaction that follows, forming the aluminum alloy and then the breaking into aluminum, gallium, and electrons (hence the current spike). The drop off represents the slow decline in accessible aluminum alloy to break apart.

3.3 Battery Analyzer

Testing on the Gough configuration and our battery cell were run using the BA500WIN Battery Metric analyzer. This battery analyzer is a modified MC2020 model and is the same analyzer used in the previous four MQPs. Additionally, the battery metric model which was used is capable of charging and measuring at low discharge voltages and currents. The BA500WIN software program Ver. 1.25 was used to control and take data from the battery metric analyzer. Data from successful tests runs was automatically saved to Microsoft Excel to be later analyzed. With the saved Excel spreadsheets, current plots would be compared to the published one in the Gough paper.

3.3.1 Tests on Gough Configuration

A three-step program was created when testing the Gough configuration. The “Battery Type” chosen was “Nickel-Cadmium Battery” which was used during a charge cycle. Using the

same settings as previous MQPs, 1 battery cell is selected with a capacity of 1,000 mAh. The first step was set to charge at 0.1 mA for 60 seconds. The second step was set to discharge at 1 mA for 30 seconds with a cut-off voltage of 1.5 V, followed by a 15 second pause step. Due to the melting point of gallium, we needed to keep the cell above 30 degrees Celsius. To accomplish this, we used an incubator set to 30-35 degrees Celsius that was in Professor Teixeira's lab.

3.3.2 The GaNTS cell, its differences to 2020 MQP, and the proposed tests

For the GaNTS cell we needed to utilize far more of the battery analyzer's capabilities. We ran a polarization program, A discharge/charge program at 30 min and 1-hour intervals, a long discharge for capacitance, and a charge program to determine rechargeability and if the gallium-to-gallium oxide reaction was reversible. The battery was chosen as "Nickel-Cadmium Battery" during any test that needed the battery to recharge or charge while long discharges were "non-Rechargeable." All tests were assumed to be "1 cell" and 1000mA capacity.

The module design was built with flexibility and transparency as core characteristics. Because the goal of this study was to notice any visual trends in surface changes, the anode and cathode had to be exposed as much as possible during each of the proposed tests. This led to a few issues in terms of ion transfer path which was much larger than the 1 or 2 separators thickness the 2020 MQP worked with, we were well equipped to see the hidden interface between the separator and gallium. Figure 22 shows that our module had the same constituents as the 2020 MQP and the same electrochemical theory driving its battery-like characteristics.

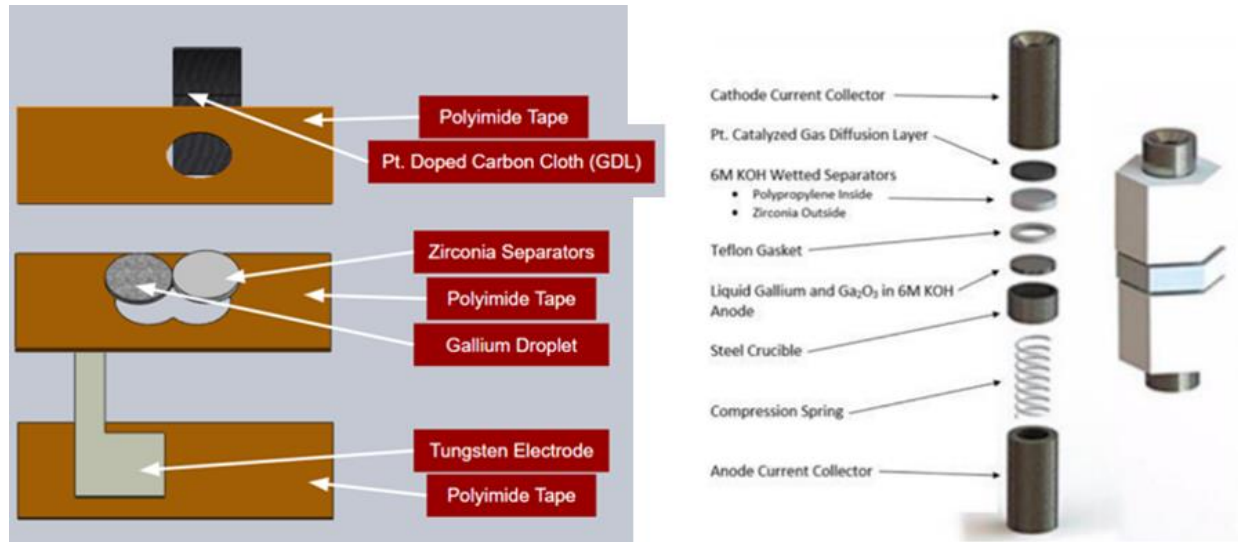


Figure 22. Comparing our final GaNTS Design to 2020 MQP Swagelok Cell

3.4 Video and Image Processing

3.4.1 ImageJ

For the second part of the Gough paper diagram, we must find the velocity head of Galinstan as it moves through the channel. To get this data from our video, we used an Image editor process ImageJ which allowed us to measure distance changes over time (videos were saved as a series of frames and with a known frame rate, you can get time displacements). By identifying the velocity changes over time in our video recordings of each trial in conjunction with excel spreadsheets saved from the battery analyzer, we can make easy comparisons between the Gough paper's configuration with aluminum and runs done without aluminum set up with a Battery Analyzer. For the GaNTS cell, we used ImageJ to calculate the surface area in the contact region between the separators and the gallium droplet. This was to calculate the current density for each GaNTS model.

3.4.2 USB Celestron Microscope

To record videos and take images, we needed to utilize a USB Celestron Microscope. This microscope allowed us to take high quality images and videos of all aspects of the battery and record the various surface changes that we would develop our conclusions from.

4. Results

When we gained access to the lab at the beginning of B term, our results were focused on how small deviations moving top down from the Gough configuration and the previous MQPs could help us create a new battery configuration. The following sections will outline how we took incremental changes from the Gough paper configuration and built our own functioning battery cell.

For convenience to the reader, we will aptly name the two reservoirs, “Reservoir A” and “Reservoir B.” Reservoir A is the one containing the Galinstan droplet while Reservoir B is the one that is open to the air with silicon. Because the terms anode and cathode change based on charging and discharging with the battery analyzer, naming conventions will be put in to help avoid confusion. Figure 22 highlights what these two reservoirs look like in our finished cell configuration.

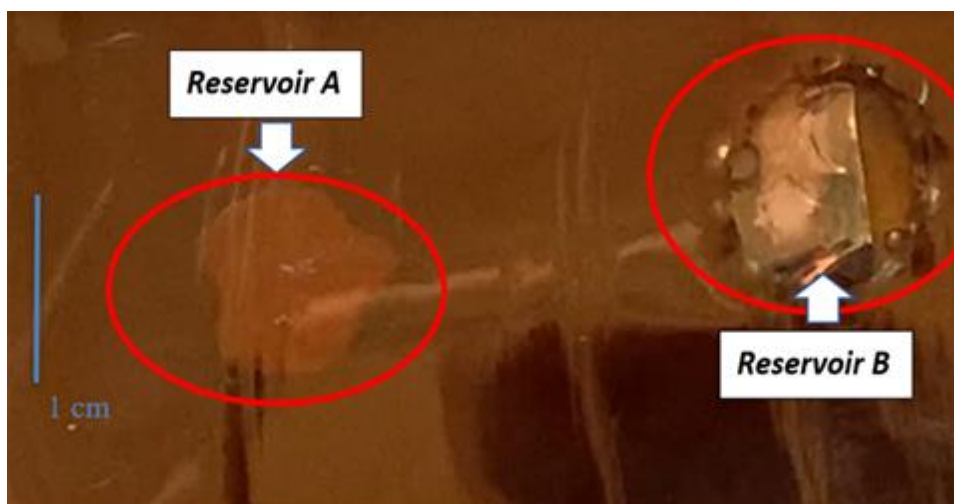


Figure 23. *Reservoirs A and B in the Gough configuration for visualizing self-actuation*

4.1 Our Gough Configuration results without aluminum

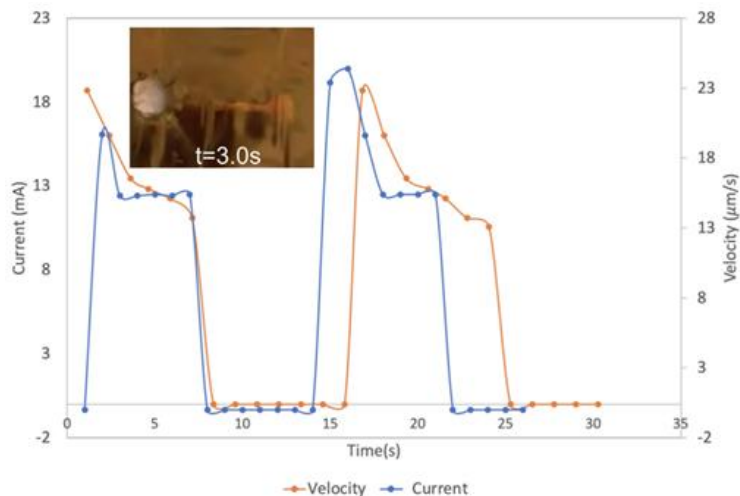


Figure 24. Our results when reproducing the Gough paper self-actuation test. The results are comparable to the published results found in Figure 21

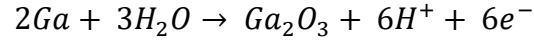
After successfully constructing the battery cell, we used the battery cell program described above to produce values for both current and velocity to recreate the graph shown in figure 23. When compared to that of the Gough Paper, the overall shape of the graphs was similar despite obtaining different current and velocity values.

When we were able to get on the same relative results for a current vs. velocity chart, we then became confident in further investigating the phenomenon of “self-actuating.” Similar shape suggests that the reaction mechanism inside the module, in terms of anodic and cathodic reactions within the reservoirs and different electrolytes without the aid of aluminum but instead a charge/discharge cycle, gives us hope that a battery cell of this type was plausible. The following sections will be sections dedicated to results that help us understand different phenomena.

4.2 Anodic Reactions in both Reservoirs A and B

For the battery analyzer tests we saw reservoir A receive a charge while the battery analyzer is assumed to have promoted a release of electrons from reservoir B. This meant we focused on the potential reactions that would occur in reservoir A when an abundance of electrons was introduced. As we know, gallium oxide occurs naturally on the surface of gallium metals in water-

based aqueous solutions. The following equation is the formation equation for gallium oxide inside of a water-based aqueous solution:

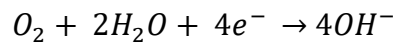
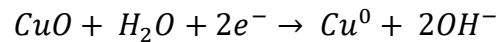


Because the right side of the equation produces gallium oxide as a product of gallium with a net charge of zero in a liquid-based electrolyte and we were introducing electrons, we assumed that reaction above was forced in the direction of right to left. This meant during the charging cycle we would see an increase in gallium with a base charge of zero and water.

Consider that with the inclusion of an aluminum flake, after alloying, a transfer of electrons happens from the aluminum stripped of its electrons to gallium cathode ions, producing base gallium too. This means that the resulting surface-tension gradient along the length of the liquid metal is a primary contributor to the “self-actuating” phenomenon that was the focus of the original gouge configuration.

4.3 Cathodic Reactions in both Reservoir A and B

While charging, the cathodic reservoir was reservoir B. The removal of electrons from an open-air reservoir housing primarily electrolyte is done through two main reactions:



Both reactions eat up a hydroxide group either with the aid of copper or with the aid of oxygen air. The inclusion of silicon was to allow oxygen to move in and out of the module, but this also caused its own set of issues. In figure 24, Reservoir B has a giant oxygen bubble form upon the charging of the module.



Figure 25. *Air formation in Reservoir B*

The copper strip became a reacting agent when removing electrons from Reservoir B. With the abundance of hydroxides supplied by the electrolyte; copper oxide will form alongside electrons that can be supplied to Reservoir A (the Anode during charging). We were made aware of the formation of the copper oxide due to the cathode's surface becoming darker in color as the charge was applied. The physical confirmation given by the darkening of the copper strip helped prove the point that the reaction between the copper strip and hydroxide is where electrons are produced.



Figure 26. *The photos above show the copper oxide formation in the electrode helping to deduce the flow of electrons.*

Seen in the left side of the figure above, the copper electrode is shown before the module was applied to the battery analyzer. The right side of the figure shows the copper electrode while the charge was being taken from Reservoir B to Reservoir A from the battery analyzer. Because of the inclusion of copper oxide in Reservoir B, the assumption is electrons are being taken from Reservoir B (the anode) and sent to Reservoir A (the cathode).

4.4 Making the GaNTS Cell

For reference the module design utilized for the first few polarization tests was not optimized. An expanded image of the inside of the module is seen in figure 26. Section 4.4.1 expands on determining the correct gas diffusion layer (GDL). Section 4.4.2 highlights the gel electrolyte and why it was unable to fix leakage issues from our precursor Gough configuration. The tungsten electrode lead under the GDL resulted in far lower initial voltage readings when the battery was hooked up and gave less consistent polarization curves. Resistance checks across portions of the battery are in section 4.4.3. Our final GaNTS cell design was built in Section 4.4.4.

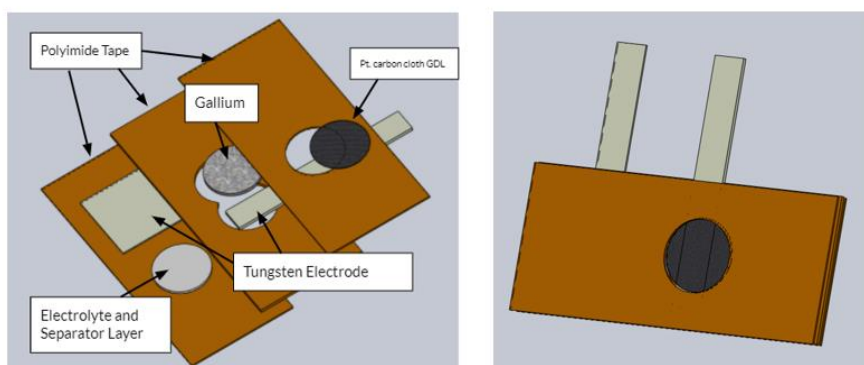


Figure 27. *Expanded Module with Tungsten Electrode connection to Cathode*

4.4.1 Determining the GDL

In our drawer of materials from previous MQPs, we had two different Pt. doped style carbon gas diffusion layers (GDLs). One was a classic Pt. doped cloth GDL that has been previously used by the 2020 MQP, the second was labeled “Pt. Catalyst”. The rigidity of the second allowed us to see the effects of oxygen permeability on the system. It is important to note the surface area between the gallium and separator for the Cloth GDL test module was 0.0396 cm² and for the graphene GDL it was 0.0225 cm².

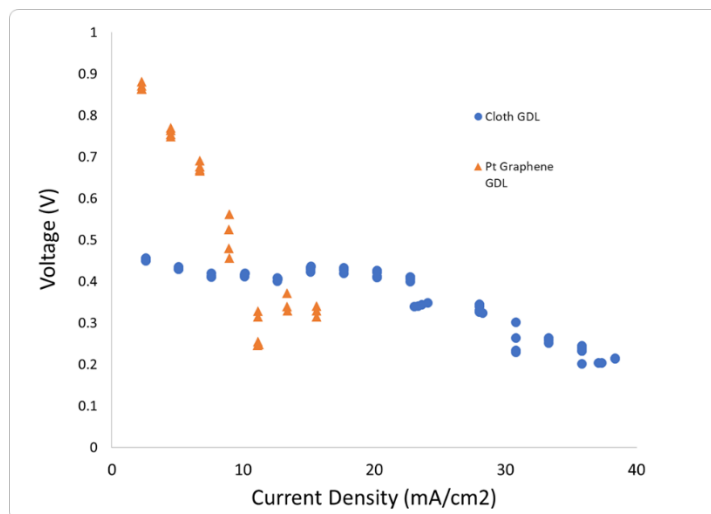


Figure 28. Comparing GDL polarization performance

Based on the findings in figure 27, the need for oxygen permeability had a significant impact on the ability for the module to survive at higher current densities. The module in figure 26 was not optimized as seen by the low voltage. Resistances across the module configuration were done to find a way to optimize the module.

4.4.2 Gel Electrolyte

Outside of GDL type, we were also curious as to the potential application of a gel electrolyte. During our tests of self-actuation in the gouge configuration, KOH leakage was a huge problem. To address these issues, we looked to the potential application of a poly-acrylic acid-based electrolyte gel. The calculations that create the gel are found in Appendix D. For modules with the gel electrolyte, the separators and the KOH are replaced with a film of electrolyte 1mm thick. Various tests were run with the gel electrolyte, but the current density far underperformed what we were looking for. Even with the area being 1/5th the Swagelok cell, the current we could supply to the system could not be above 0.26mA.



Figure 29. Gel Electrolyte preparation

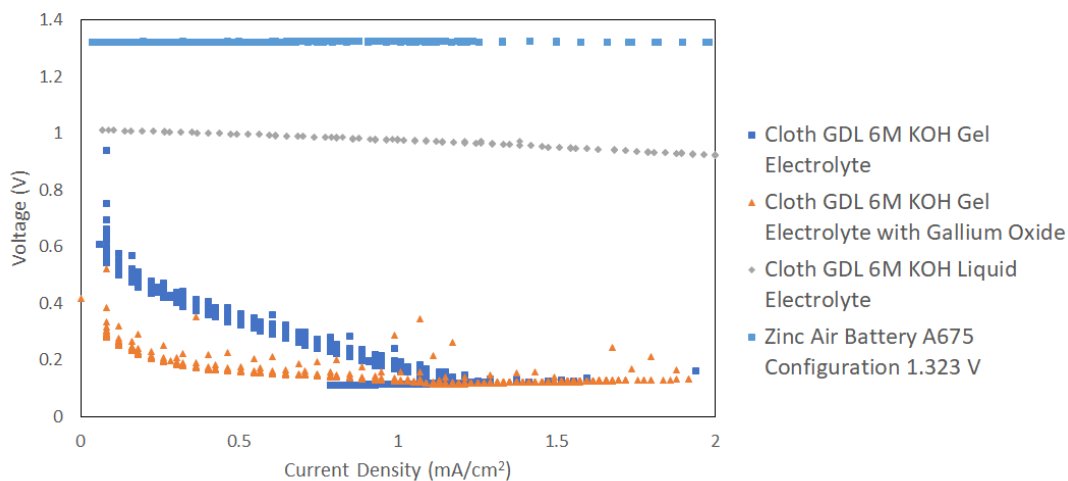


Figure 30. Comparing the effects with and without the gel electrolyte to Commercial-Grade Zinc-Air Battery

4.4.3 Module Resistance

As seen in figure 26 when determining the correct gas diffusion layer, we determined the module was performing far below an expected initial voltage of 1.3-1.0V. To solve the issue of lower voltage we wanted to determine the resistances across the sections of the configuration to see where an elevated level of resistance was impeding the current flow during discharge. Below is a table 4 of our results when measuring resistances across several key areas inside of our cell.

Table 4. Table of Resistances inside Module

<i>Interface Measured</i>	<i>Resistance</i>
Gas Diffusion Layer and Tungsten Electrode	0.4Ω
Liquid Gallium and Tungsten (Note that Gallium Oxide was present at interface)	0.2Ω
GDL and 6M KOH-Soaked Separator	0.0Ω
Module with Tungsten to GDL Electrode connection	0.3Ω

Based on the resistance results, we knew the GDL to tungsten electrode interface was causing issues for the modules voltage output. This correlation resulted in us remodeling the cell's configuration to get a more accurate polarization curve.

4.4.4 Building Our Final GaNTS cell

Our final configuration design was made by removing the tungsten electrode from between the separators and GDL. By giving the current a straight path from the GDL to the electrolyte, rather than creating an opportunity for the current to bypass the GDL, we can assume the forward reaction due to oxygen was increased giving us a higher voltage. The readouts from the multimeter of 1.1V with 0L of resistance are shown in figure 30. The “0L” readout means infinite resistance. This reading was taken from a spent module when a long discharge was completed. This highlights the high resistance the module will have when excessive gallium oxide formation coats the anode.



Figure 31. Voltage and Resistance check with new Configuration.

Once the configuration was optimized for resistance by changing the route of electrons in the cathode, we started comparing it to the Swagelok configuration of the previous MQP. In figure 31, we compare the final GaNTS design to the Swagelok cell of previous MQPs. This comparison highlights that the components that make up the cell are identical.

After confirming that the only difference in the cell is its configuration, we set up a Swagelok configuration of our own for comparison. The modules were both held at 45-50°C and run under increasing currents to determine their polarization curves. The difference in mA ranges is due to the areas of both the Swagelok and flat configuration differing by a ratio of 5:1, respectively. The comparison of the two are in figure 32.

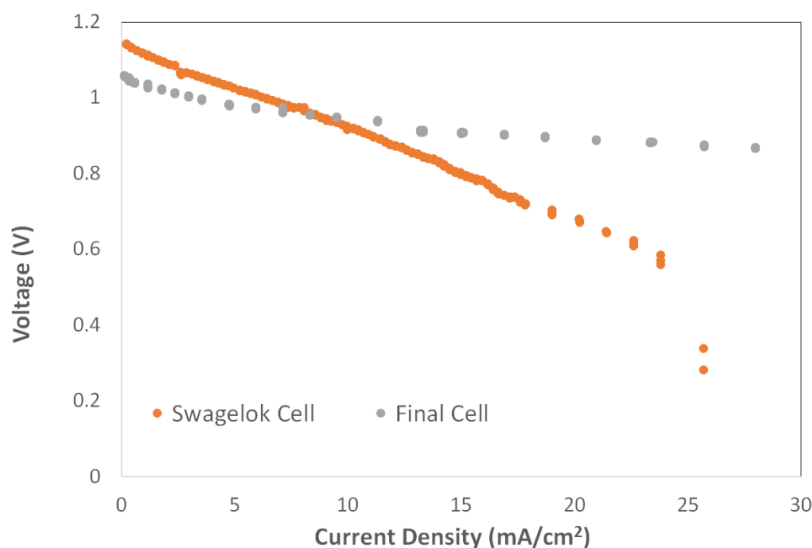


Figure 32. Comparing polarization to Swagelok configuration

4.4.5 Comparing Polarizations over a longer range of Current

Figure 33 is a table of three polarizations run with the same GaNTS module and area. Figure 33 highlights that the polarization of the cell is very consistent and reproducible considering the materials for construction. A polarization curve can show us where the cell can comfortably operate. In figure 33, the three polarization curves show a current density decrease (due to internal resistance formations from gallium oxide over time). The surface area calculation was done based on the surface contact between gallium and the separators, but a case could be made for the surface area of the gallium droplet instead. For all polarizations the open circuit voltage (OCV) was 1.23V.

It is important to note that if the battery operated with respect to the total surface area of the gallium, then the battery's internal tendency to create resistances whether from evaporation because of temperature in the incubator or the formation of gallium oxide is a major factor in the sustainability of the configuration. While our configuration is optimized for visibility, the main goal of this configuration was not performance.

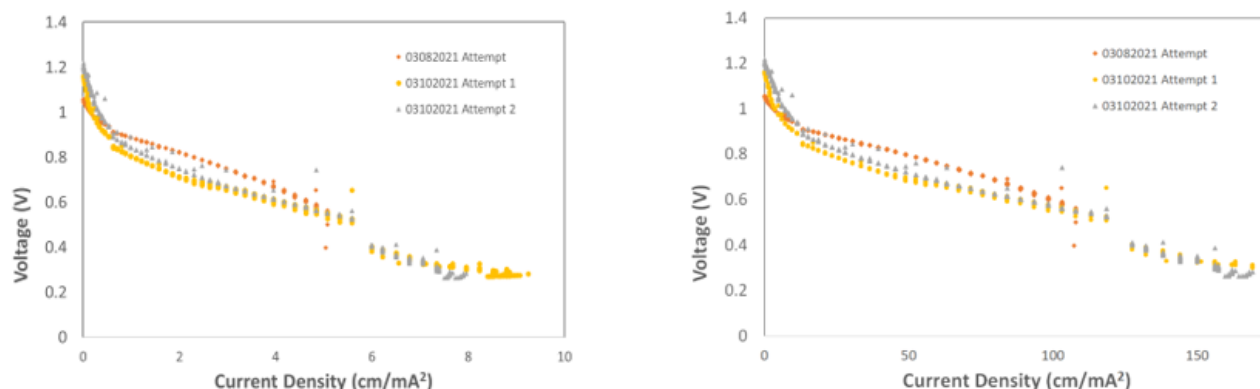


Figure 33. Comparing polarizations for reproducibility. **Left** shows the current density if the surface area is considered the total surface area of the gallium droplet due to the no slip boundary clause **Right** shows the current density calculation if we consider that ion transfer of gallium happens only along the boundary of gallium and the separators.

4.5 Discharge Cycle

4.5.1 Our Best Discharge Results

The battery analyzer program used to test the GaNTS configuration's ability to discharge was first based on programs used in previous MQPs. However, after running a few failed tests we realized that our cell did not have enough stability to be comparable to previous years. Throughout our experiments, we found it difficult to recreate discharge times to compare to previous years and found that our cell would hit a 'failure' point where the cell would become unstable and voltage readings would become inconsistent. We believe this is due to the smaller surface area and the heightened effect of gallium oxide production along that area. When the area is smaller, the gallium

oxide will form faster and therefore the battery will begin to short. This became especially apparent during discharges through the visibility through our cell. All discharge tests we run with a 0.1V cutoff and a 10-minute pause at the beginning. This section includes a few discharge curves which we found when trying to get comparable results to previous MQPs.

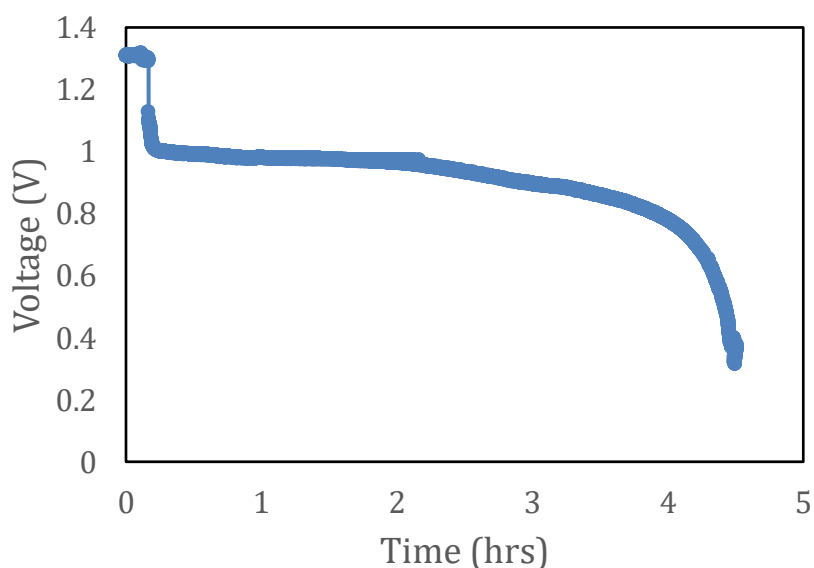


Figure 34. *GaNTS cell discharge curve at 50 °C and 2.45 mA/cm²*

In the discharge curve in figure 34, we got a resulting discharge time of around 4 to 4.5 hours before hitting a failure point at which the voltage readings started to become unstable. This test gave a current density of 2.45 mA/cm², making it one of the best results we had in terms of stability. However, many of the tests we ran resulted in unstable discharge curves. Through the transparency of our cell, we were able to determine a few possible reasons why our discharge curves were inconsistent. We believe that the main issue causing the inconsistencies is the electrolyte either evaporating in the separators or leaking through the polyimide layers. This became especially apparent since there was 1.092g of KOH at the start and at the end of the test, the KOH weighed 0.148g, resulting in an approximate loss of 0.944g of electrolyte.

4.5.2 Reproducibility of Our Discharge Curve

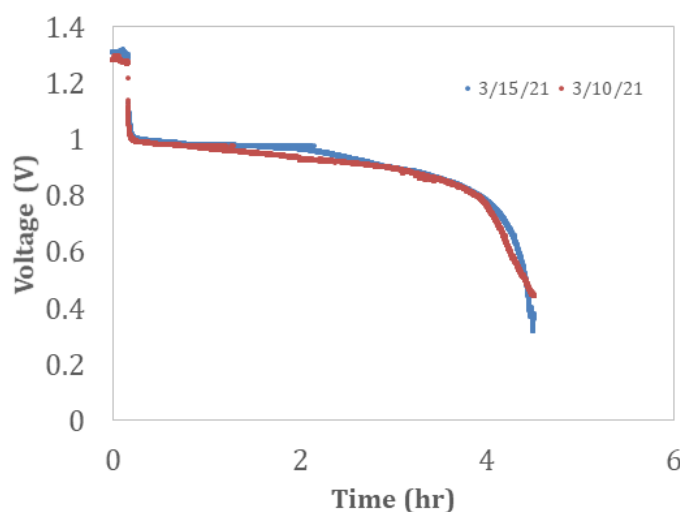


Figure 35. Showing reproducibility of the results of our best discharge curves both run at 0.5 mA

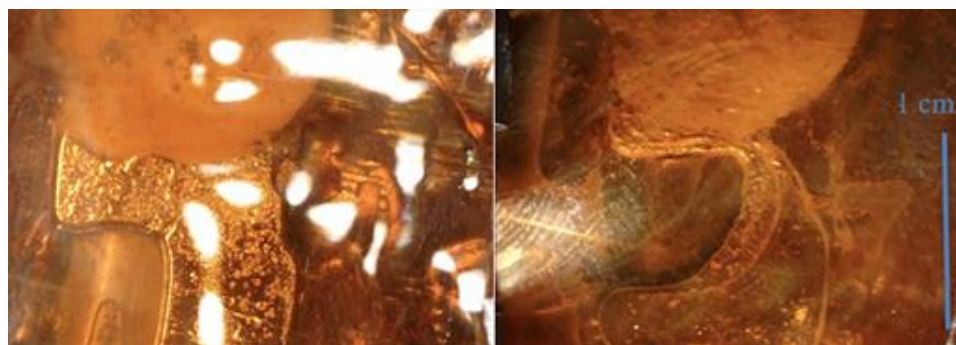


Figure 36. Left. Before 4.5-hour discharge **Right.** After 4.5-hour discharge from 3/15/21

Additionally, we wanted to make sure that these results were reproducible and consistent to make sure our cell was reliable. The graph in figure 35 compares our two most successful discharge curves. As you can see, the discharge curves almost line-up exactly and both give a current density of around 2.5 mA/cm^2 . This evidence proves the GaNTS cell's ability to consistently discharge and that these results are reproducible. Furthermore, through the transparency of our cell, we were able to visualize the anode and cathode which clarified a few things. First, contact surface between the gallium and the separators is necessary for discharge to occur. As you can see in figure 39, at the start of the test the gallium had complete contact with the separators, and at the end, despite drying up of electrolyte and the physical movement of

gallium, there is still a complete connection between gallium and the separators at the end. Second, at the contact area, there are visible differences which indicate the formation of gallium oxide (Ga_2O_3) which in its purest form is white powder. In the test from 3/10/21, we started with .986g of gallium and ended with 1.099g, indicating that potentially 0.014126 moles of gallium reacted to make gallium oxide. Both issues contributed to the failure of the discharge test and should be addressed in the future.

4.5.3 Discharge curve of GaNTS cell using NaOH Electrolyte

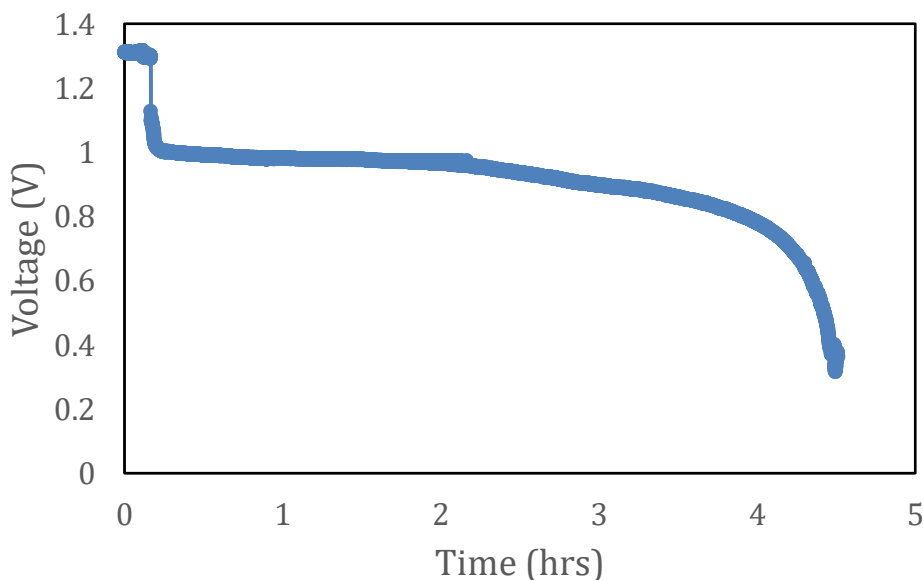


Figure 37. Discharge curve using NaOH electrolyte. NaOH electrolyte was able to run slightly longer before failing but displayed instability throughout the test run.

We also decided to run a test using NaOH to see if changing the electrolyte had any effects on its ability to discharge. Figure 37 shows the resulting discharge curve which was able to run for 7 hours. Although this test shows some inconsistencies, it does prove that NaOH could be a viable option as an electrolyte in the GaNTS cell. Compared to tests run with KOH, the failure point was around 5 hours instead of 4 hours, which shows an NaOH electrolyte could potentially last longer than a KOH electrolyte. However, the starting voltage was only around 0.8V, which is 0.4V lower than that of our results for the KOH electrolyte. Overall, this test displayed a promising potential

for NaOH to be used as an electrolyte, but further investigation and testing needs to be done to validate this.

4.5.4 Orphaning withing the GaNTS Configuration

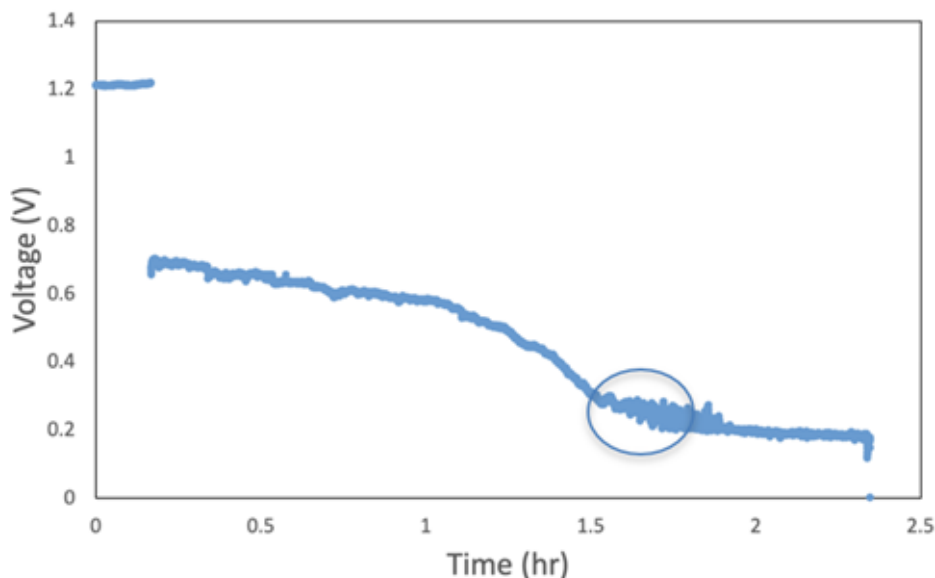


Figure 38. Discharge curve for 4/1/21 run. The circled area above indicates where we believed chemical orphaning was taking place. See Appendix A Video 3 to view this test run.

This test was run to try to match the current density achieved by the previous MPQ in 2020. To do this, we used the contact area between the gallium drop and separators ($.234\text{cm}^2$) to calculate the current needed to achieve 7.99 mA/cm^2 current density. This calculation gave us a current of 1.87 mA to run the discharge until failure. Although this test did not run as well as other runs, it did reveal some possible issues occurring within the configuration. We believe what could be happening is called chemical orphaning, which is when a metal becomes electronically disconnected from the current collector while the ionic connection with the electrolyte is maintained [32]. This could potentially prove that gallium oxide deposition in the separators. The circle in the graph in figure 38 indicates the point at which the orphaning may be occurring. As you can see, the instability starts to occur between 1.5 and 2 hours, then starts to decline until failure. During this time, the gallium still has complete contact with the separators which makes

us believe it became electronically disconnected but was still able to maintain contact with the electrolyte through gallium oxide deposition in the separators. However, this finding was discovered late in the project and needs further investigation to confirm.

4.6 Discharge-Charge Cycles

4.6.1 Testing for Rechargeability and Stability

Using the results from the battery analyzer, we determined the GaNTS configuration does have the partial ability to be partially rechargeable. To demonstrate rechargeability, we ran discharge then charge test cycles. We ran these tests with multiple cycles, (2 discharge and 2 charge cycles) and had a few variations of the test. We originally ran the discharge/charge tests with 60-minute intervals and ran at a discharge current of 0.5 mA. However, once we attempted to run tests, we realized that the GaNTS cell did not have the capacity to run for longer intervals. The graph of our failed 60-minute interval discharge/charge can be seen in figure 39. This test revealed a critical issue the GaNTS cell was experiencing.

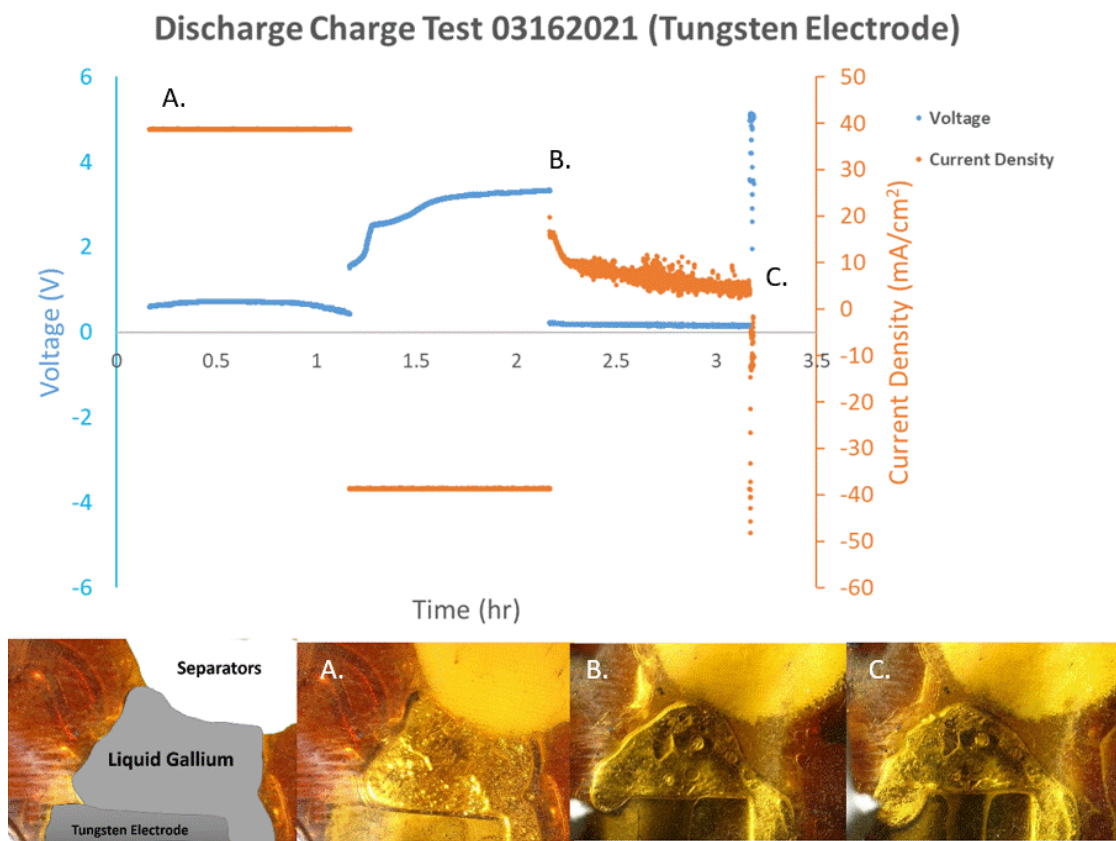


Figure 39. Failed discharge/charge test on second discharge cycle. Pictures A., B., and C.: Change in contact area between gallium and separators (anode and cathode) shows failure method. Liquid KOH electrolyte evaporation shown by receding liquid front on the tungsten electrode and in layers of polyimide between images B. and C.

a) Pictured in a is the contact between the gallium and the separators at the beginning of the experiment. The gallium has complete contact with the cathode side which shows a higher voltage reading of 1.1V. b) At the start of the second discharge, the gallium contracts away from the separators, causing the configuration to start shorting. c) Complete test failure due to no contact between the gallium and the separators. This was an important visualization of the contact area because it proves that the gallium must have contact with the cathode side to discharge and charge. When there is more contact between the gallium and the separators, the configuration is more stable and able to hold a charge. It should be noted that the GaNTS cell was discharging between 0.4V-0.7V on the first successful discharge cycle and charged up to 3.3V.

The next discharge/charge test we ran was an alteration of the first attempt. As previously stated, the GaNTS configuration was not able to stabilize during 60-minute cycles. So, we decided to change the program settings to 30-minute intervals which proved to improve our results. This test was also run at 5 mA discharge current and two 10-minute pauses at the start and finish.

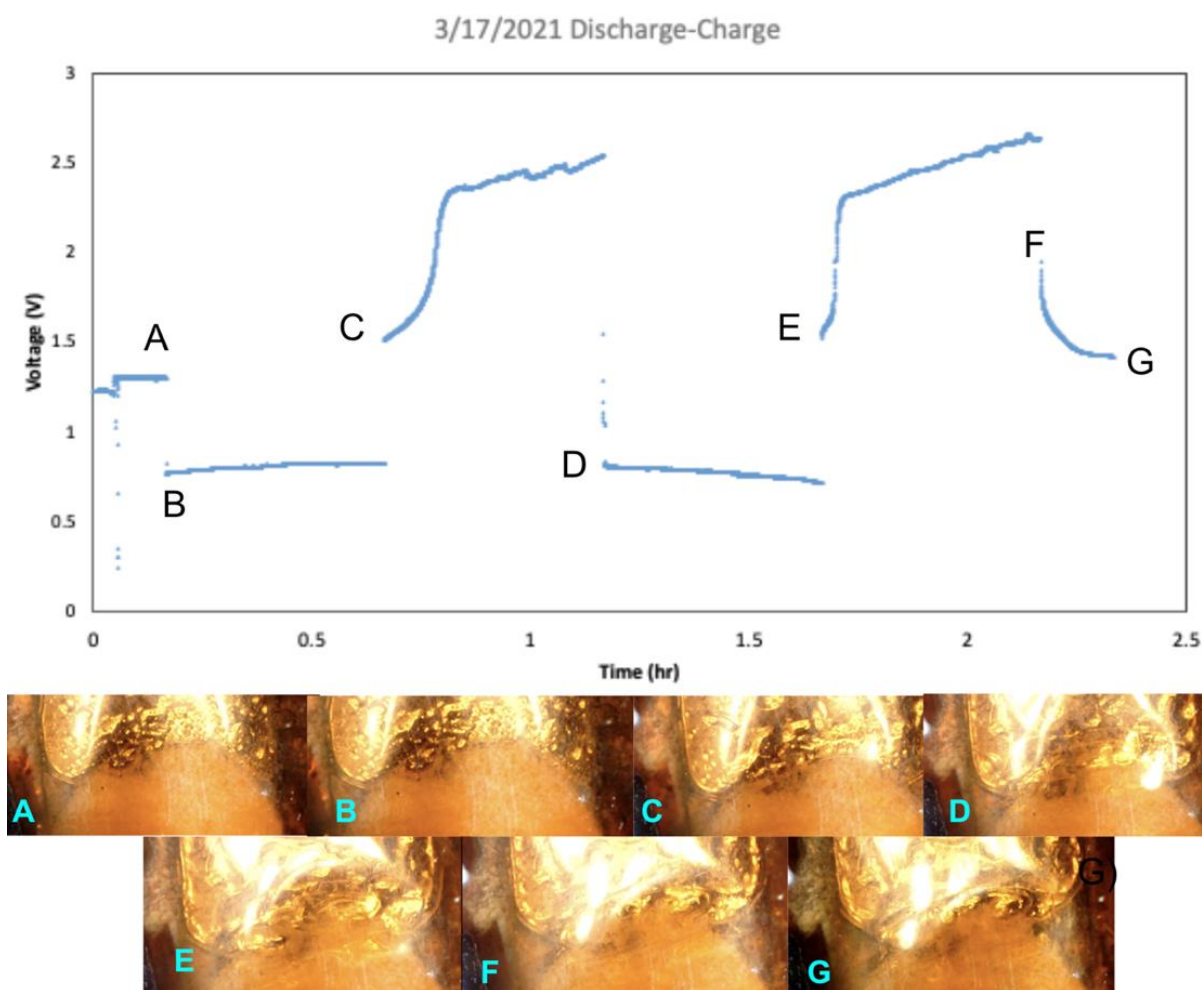


Figure 40. Discharge/charge cycle at 5 mA current with 30-minute intervals. Each picture represents the start of a cycle and shows the differences overtime.

Figure 40 is the graph of the successful 30-minute cycle test. This run was able to complete all six cycles with very consistent readings. **a)** The contact between the anode and cathode was at a max during the pause step and gave a voltage of 1.3V at the start of the test. **b)** Contrasting from the failed run, the gallium maintained its contact with the separators and was able to hold a charge of

1.3V after the final 30-minute charge cycle. the failed run, the gallium maintained its contact with the separators and was able to hold a charge of 1.3V after the final 30-minute charge cycle.

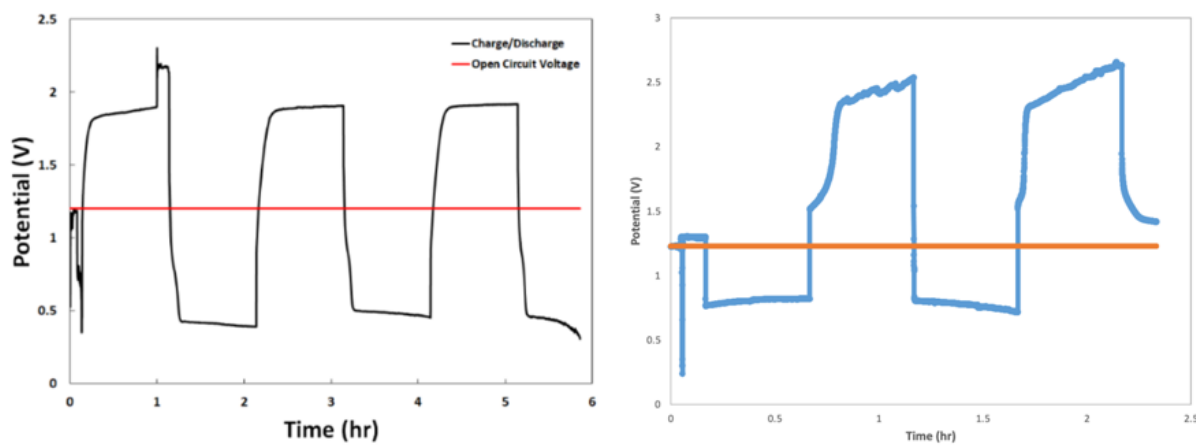


Figure 41. Potential vs. time graph for discharge/charge. *Left.* 2020 cell *Right.* GaNTS cell

This run had the most consistent results and was able to hold a charge of 1.3V for the 10-minute pause. These consistent results prove that the GaNTS configuration does have the ability to be rechargeable and how the cell is able to stabilize. Furthermore, our cell was able to charge at a higher voltage and was able to hold a higher charge than that of the cell from 2020. This shows our cell's potential to hold more charge and discharge at a higher voltage. Figure 41 contains the graphs of the successful runs from our cell (right) and the cell from 2020 (left). It should be noted that our results were for 30-minute cycles which is half that of the 2020 results which were with 60-minute cycles. Our charge cycles also increased in voltage over time which differs from 2020 which show consistent results for the whole hour charge. This indicates that our cell has yet to hit its potential max voltage. The 2020 cell charged at a max voltage of 1.8/1.9V, but our GaNTS cell was able to charge above 2.5V and shows potential to be even higher. Further alterations to the configuration would help with the overall stability and improve its ability to discharge and charge with longer cycles.

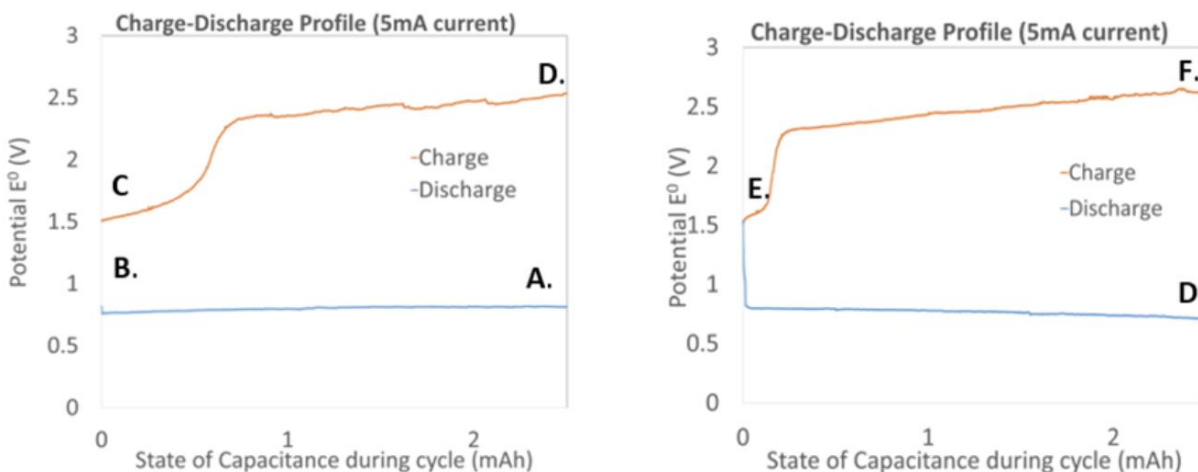


Figure 42. Comparing the Charge Cycles from the 03/17/2021 Discharge-Charge Test

Figure 42 compares the charge and discharge life of both the first and second cycle from our 03/17/2021 test. The only noticeable difference we see is the speed at which the battery bounces back up towards its max potential. Note that both are abbreviated cycles and do not show the full discharge or charge of the battery. Getting a full cycle of the GaNTS cell adds a vulnerability to other failure points that the module could not handle. The main reason being the gradual separation of the gallium and electrolyte-soaked separator that can be seen in figure 39.

4.6.2 Testing with a Stainless-Steel Electrode

We also decided to run the original 60-minute program on the GaNTS cell but using a different electrode. Instead of using tungsten as the electrode, we used a strip of stainless steel. Looking at the program report, we could see that the SSE (stainless steel electrode) proved to improve the results. The configuration with the SSE was able to run through the program completely with the 60-minute cycles and reach a max charge of 3.5V. Additionally, during the

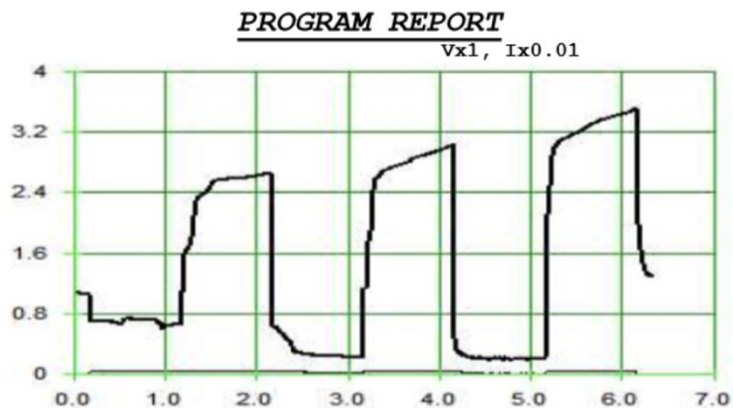


Figure 43. Program report of discharge/charge test for cell with SSE

first discharge the cell was able to discharge around 0.7V, but on the second and third cycles the discharge dropped to 0.2V. Due to the discharge dropping low during the second and third cycles, we believe the cell was experiencing further resistance changes as the charge/discharge cycles repeated. We associated this resistance increase with the excessive leaking the thicker SSE electrode caused the cell to have. It should be noted that stainless steel is actually quite resistive and would not work for high power applications. Additionally, this test was only run once and additional testing on the cell may point to stainless steel as the better electrode option.

4.7 Charge Cycle and Gallium Production

4.7.1 Control Test (Water Only)

To understand other tests, we needed to have control data. For this test, we used a petri dish setup and shown in figure 44 but replaced the KOH with distilled water.



Figure 44. Example of petri dish configuration

The test was set to run for 1 mA for a 30-minute charge. This test demonstrated how rapidly electrolysis happened in the water-only test with the video (Appendix A: Video 5). We can presume these bubbles to be hydrogen gas. During electrolysis, the cathodic reaction (which in a charge cycle is the tungsten strip) is assumed to produce Hydrogen air and negatively charged oxygen ions. These oxygen ions when traveled to the anode (in this case the GDL) will reform into Oxygen air and produce the electrons that will be resupplied to the system.

Cathode Reaction



Anode Reaction



In the first test shown in figure 44, the pH of the water was initially recorded at 7.3 but as the test concluded, it was recorded at 9.69. From our calculations, the number of moles of OH that

were introduced into the system were 6.485×10^{-17} . Therefore, we produced 103.3 mA from the following equation: $\text{O}_2 + \text{H}_2\text{O} + 4\text{e}^- \leftrightarrow 4\text{OH}^-$. The potential (E°) for this reaction was determined to be 1.23 volts [33].

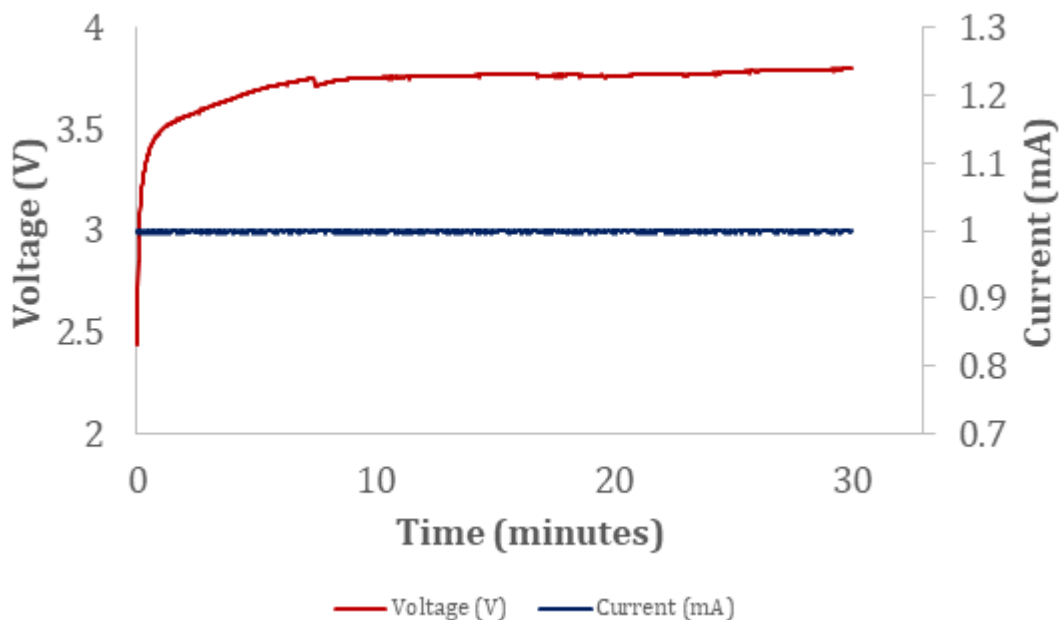


Figure 45. Shows the voltage and current vs time for the water only test.

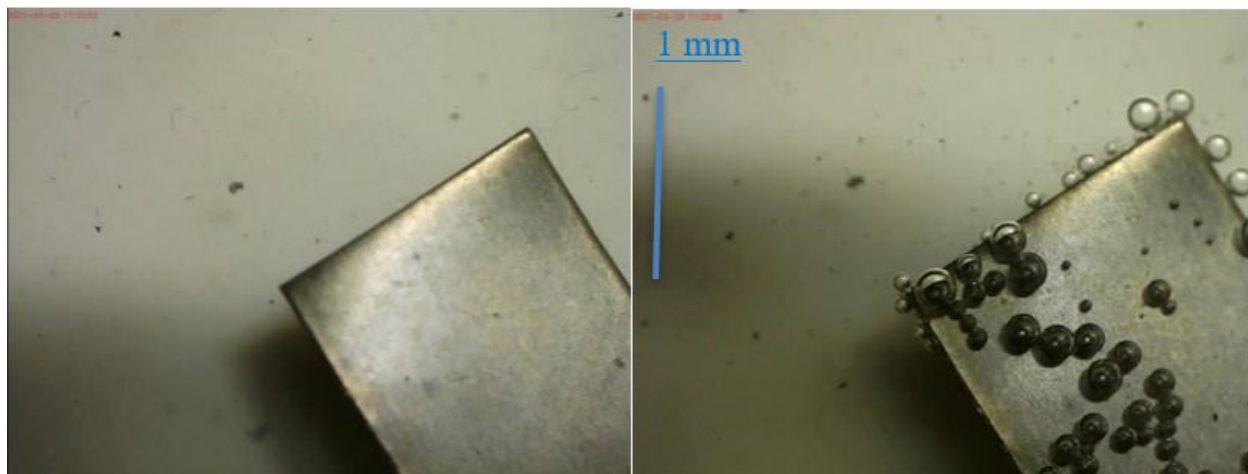


Figure 46. Left. shows the tungsten electrode from water only test just after program began. Right shows the tungsten electrode from water only test as program is about to end

4.7.2 Control Test (KOH Only)

We ran the same program as the previous tests with water only. For this test we used KOH without gallium oxide acting as the electrolyte instead of water. The photos taken during this test

(figure 48) for this test shows a noticeable decrease in bubbles as opposed to the photos taken from the water only test as shown in figure 46. The KOH only control test peaked at 2.187 V compared and 5.101 V for the water only control test. We could not measure the pH however due to it being above 14. The graph in figure 47 is representative of the other tests we ran with KOH. The potential (E°) for this reaction was determined to be 1.23 volts [33].

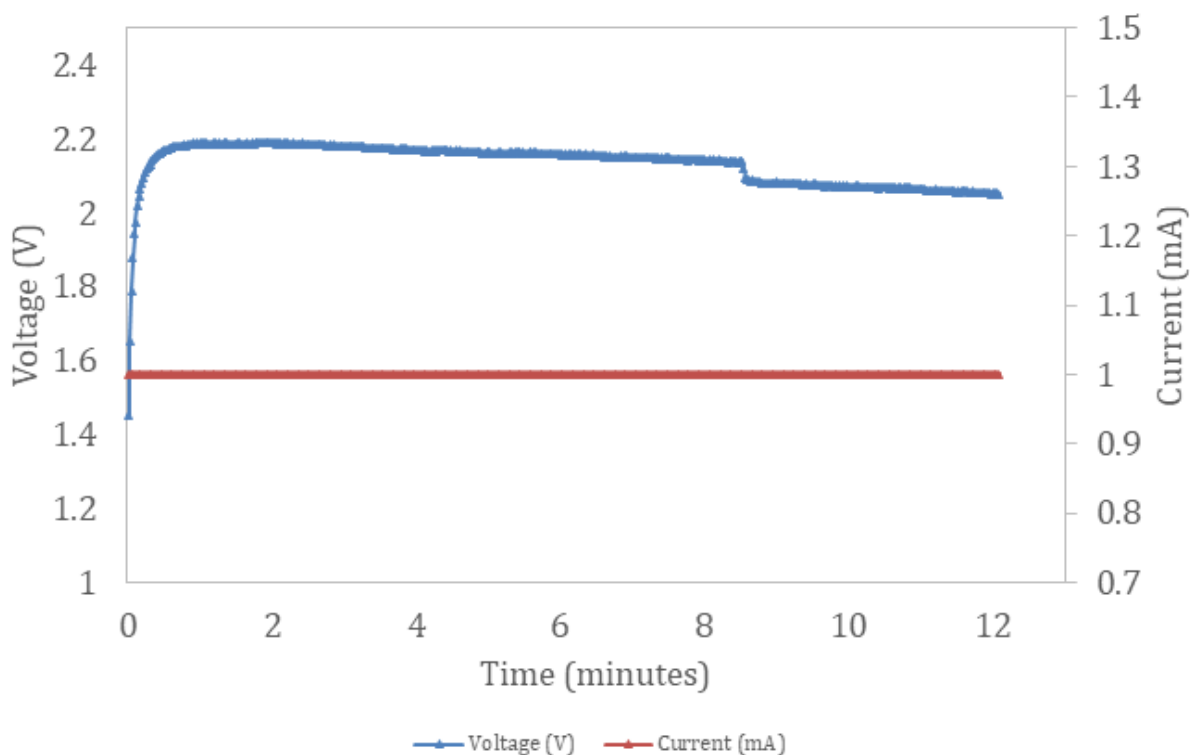


Figure 47. Shows the voltage and current vs. time of the KOH only charge test

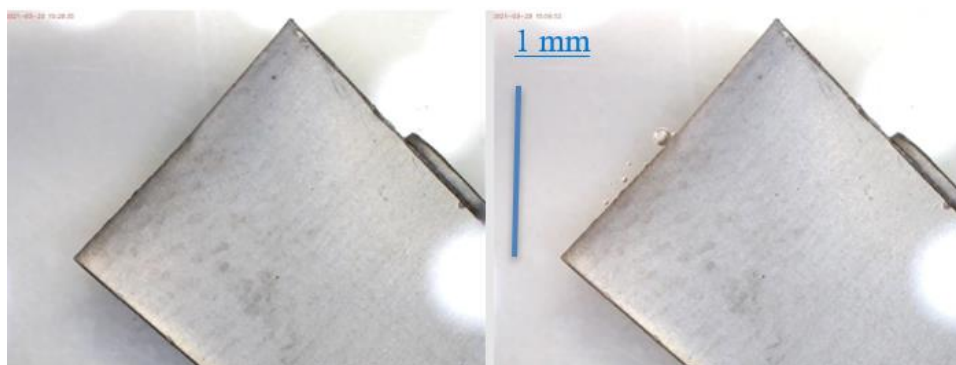


Figure 48. Left. tungsten electrode from KOH only test after program began. Right. tungsten electrode from water only test as program is about to end

4.7.3 Gallium Oxide dissolved into KOH Electrolyte (1 mA)

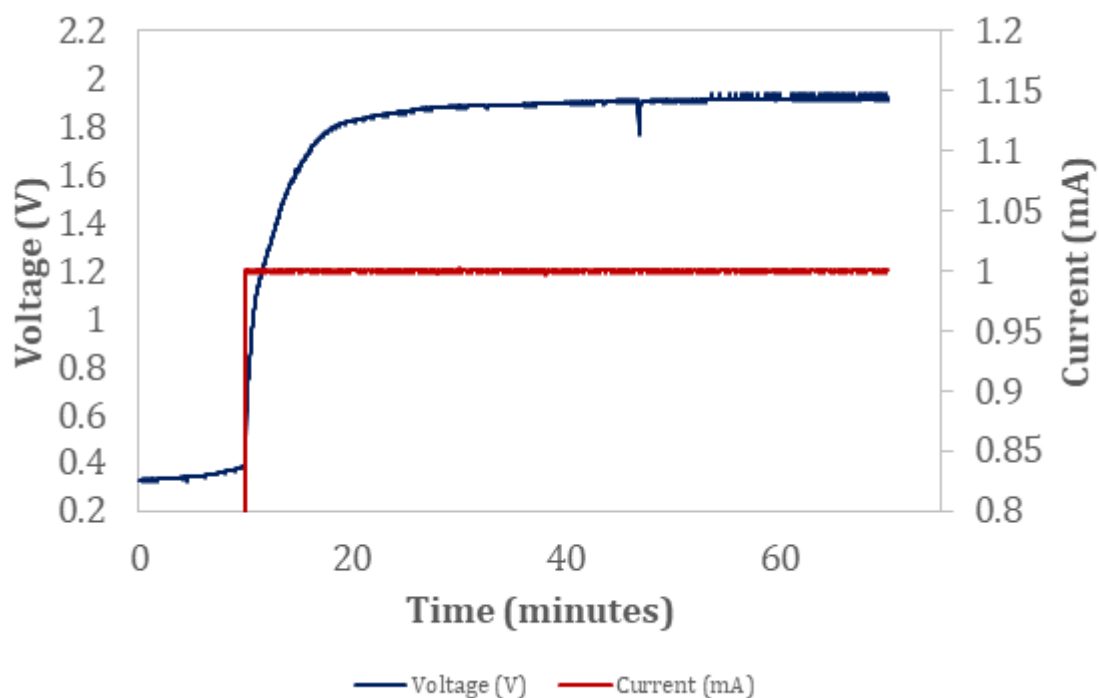


Figure 49. Voltage and Current Vs. Time Graph of 1 mA Ga_2O_3 in KOH Charge Test

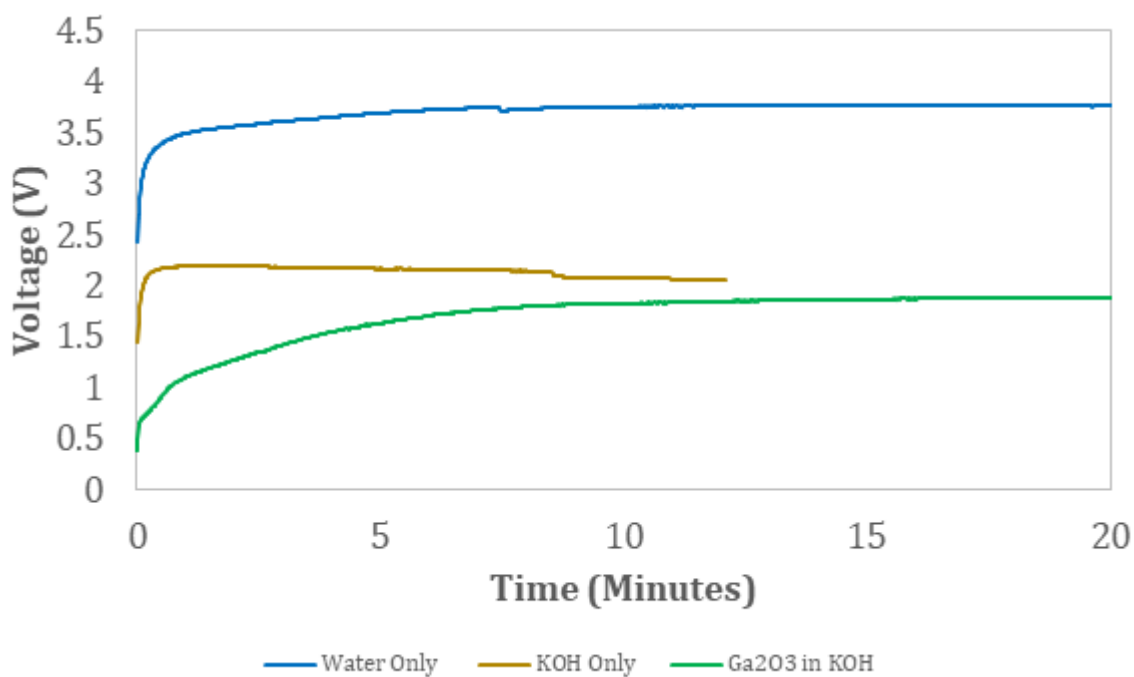


Figure 50. Shows the voltage vs. time for the water only, KOH only, and 0.001 mol Ga_2O_3 in KOH charge tests

To determine if the GaNTS cell was rechargeable, we needed to understand if gallium would form during charge when gallium oxide was dissolved into the electrolyte. To test this, we dissolved 0.001 mol gallium oxide in 10mL of 6M KOH to be used in the petri dish configuration without separators. We used the same program settings as the water only and KOH only tests except we added a 5-minute pause and ran the charge cycle for 1 hour. After running this test, we observed no traces of gallium production in the dish.

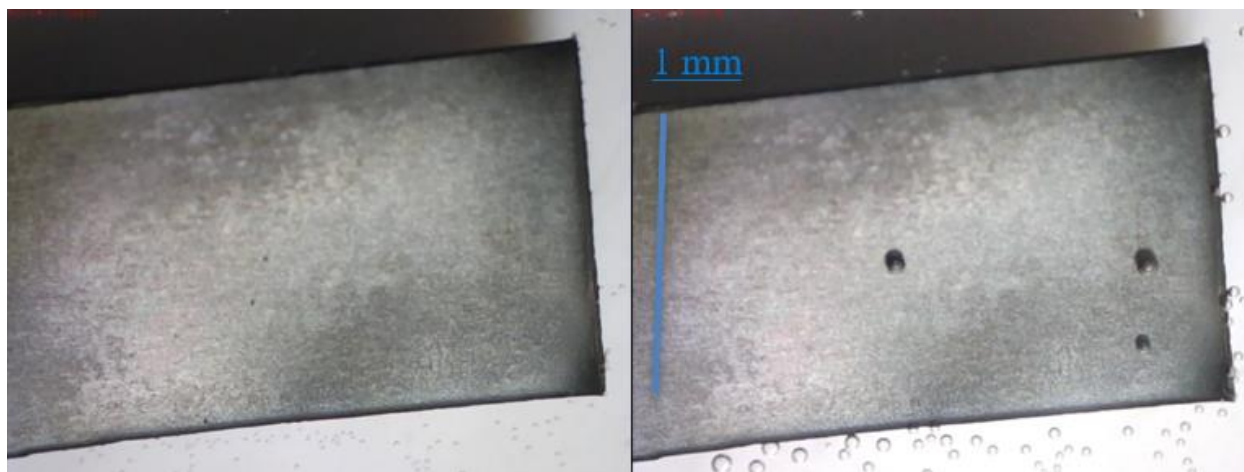


Figure 51. Left. Shows tungsten electrode at beginning of charge cycle. Right. Shows tungsten electrode at the end of the charge cycle

4.7.4 Gallium Oxide dissolved into KOH Electrolyte (5 mA)

Gallium Oxide Charge Test	Moles
KOH (measured from 6M KOH sol)	0.06 mol
Ga_2O_3 (measured from dissolved amount)	0.001 mol
Electrons (measured from 5mAh Charge test 04052021)	5.1896E-7 mol
Ga "recovered"	0.001176 mol
H_2O Lost	0.144 mol

Figure 52. Gallium Oxide Charge Test table showing mole amounts during the test highlighting how most of the gallium oxide to gallium reaction was done because of the KOH electrolyte and not the current flow during charge.

Since the previous test to determine if the GaNTS cell is rechargeable was ineffective, we decided that we needed to apply more current to the cell. We altered the program settings so that

it would begin with a 5-minute pause, then it was to charge for an hour at 5 mA. We ran this test twice, once at each side of the cell (once at GDL & once at tungsten) using the petri dish configuration without separators. For this test, we dissolved 0.192 grams of Ga_2O_3 into 10 mL of KOH for the electrolyte. This gave us a resulting solubility of 1.92g/100mL for gallium oxide in a 6M KOH solution. Before the program was started, we calculated the density of the KOH to be 1.2184 g/mL with the dissolved gallium oxide. When the program concluded, we measured a loss of 2.6 mL of electrolyte and an increased density of 1.3053 g/mL, but most importantly, we recovered 0.082 grams of gallium shown in figure 53.

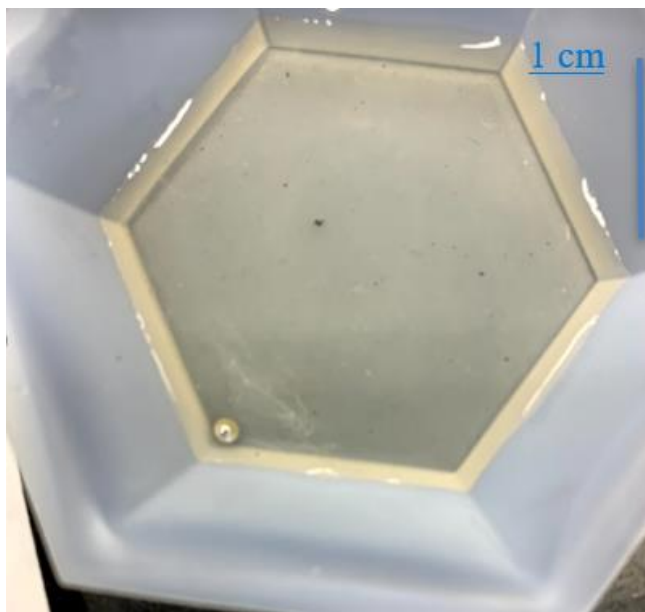


Figure 53. Shows the gallium recovered from 5 mA gallium oxide dissolved in KOH electrolyte charge test

5.0 Conclusions & Recommendations

5.1 What our project taught us

Throughout our tests with the Gough configuration, we quickly came to understand the shortcomings of utilizing polyimide tape with a highly basic solution. The electrolyte was able to easily eat through the layers of the tape and made the battery inefficient as the electrolyte would soon after lose contact with the gallium and the separators. Further analysis in the several issues that this causes for the module can be found in figure 54.

5.1.1 Leakage liquid electrolyte + polyimide

Like the previous MQP projects, we experienced many accounts of electrolyte leakage. This issue was impossible to overcome with the materials we used to construct our cells to be tested. This problem caused the KOH to flood out of the connecting channel and onto the elevated surface of polyimide to either side which would make the cell obsolete for further testing. We would then be forced to reconstruct the entire cell with a highly likely chance for this complication to reoccur. The following image is the result of excessive KOH leakage between the silicon and middle layer of the cell taken during deconstruction of a Gough configuration early in the project.

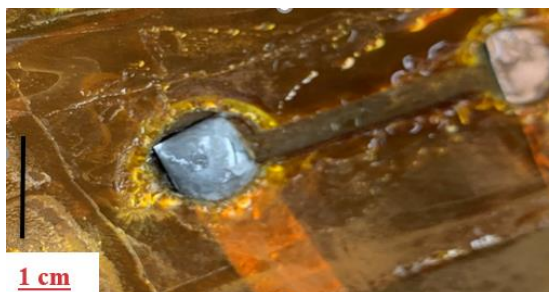


Figure 54. *Leakage after running a few cycles*

We also experienced this issue when constructing our GaNTS cell after experiencing leakage in our Gough cell. This leaking led to many issues during testing. During some of our experiments, the KOH would leak which caused the battery to short over time. In some of our

tests, we would measure the KOH before and after testing and would find that we had less electrolyte than when the test started. This may be one reason our voltage readings were so inconsistent. As the gallium loses contact with the electrolyte, the voltage becomes less consistent and eventually shorts during complete disconnect.

5.1.2 Electrode slipping/deformation polyimide tape

Another issue we had when testing the GaNTS cell and Gough configuration we created was that the electrodes would slide easily out of the reservoirs. The copper strip tape made it easy for the KOH electrolyte to leak between the layers. Once the KOH began to leak between the layers, the adhesives of both the copper tape and the polyimide would start to un-stick and eventually the layers would become unusable. Furthermore, the tungsten electrode would slip and move when connected to the battery analyzer leads due to the KOH leaking in between the layers. This would cause interference with our results and would lead us to having to reconstruct the cell from scratch. The tungsten would be stuck to the adhesive layer to keep still, however, when the KOH leaked, the adhesive would unstick which would cause the tungsten to slip. The polyimide tape caused many issues throughout this project and an alternative material may improve the overall quality and functionality of this configuration. Examples of the leakage through the polyimide layers can be seen in figure 55.



Figure 55. *Evidence of KOH leakage through the polyimide layers*

5.2 Complications during Reproducibility

The biggest issue for our project was trying to reproduce similar tests back-to-back for reproducible results. First, we wanted to reproduce the results of the Gough experiments to prove that Galinstan can be self-actuated to accelerate down a channel. Next, we wanted to make sure the GaNTS cell was able to reproduce the results of the various tests we ran throughout the project. These main tests include the polarization curves, four-hour discharge curves, and the discharge-charge curves. Being able to reproduce the results of these important experiments would prove the feasibility and viability of our configuration and take the GaNTS cell one step closer to being applicable for commercial use.

5.2.1 Required New Parts Each Test (or reusing)

Another major issue we faced was with the components themselves. As we ran tests on a fully assembled module, certain parts would require to be replaced before additional tests could be ran. After just one test, the polyimide layers, would become cloudy, which made taking photos and videos with the microscopes much less effective. The polyimide would also lose its ability to create a reliable seal around the reservoirs as the KOH would seep out during tests and erode its adhesives. Due to the heat required to keep the gallium in a liquid state, the polyimide would also

shrink and form small wrinkles on the surface layers which would also impact the process of taking photos and recording videos. Besides the polyimide, the GDL would also need to be replaced quite often as well. This was mainly because in the GaNTS configuration, we needed to attach the clips from the battery analyzer directly to the GDL which would often tear the fabric and remove the necessary platinum from its surface. Another component that was replaced after only a few tests were the electrodes. The tungsten electrode would last longer than the copper electrodes used for the Gough configuration, but would still suffer from corrosion. Finally, the separators needed to be replaced very commonly as well. As previously stated, gallium would find its way into the layers of separators which would potentially short the cell. Long-term exposure to KOH would also cause the separators to disintegrate and become like a paste, but it was much less effective in this state.



Figure 56. Shows the disintegrated separators due to long-term KOH exposure

5.2.2 Use of Gallium Required an Incubator

While Galinstan could be used to run tests in room temperature, gallium required to remain above 30° C. While the incubator was required to keep the gallium in a liquid state and served its role effectively, its use also created other issues such as an acceleration of the evaporation of KOH and the effects on the polyimide listed in section 5.2.1. Another issue that comes from using the

incubator was that increasing the temperature to $>30^{\circ}\text{C}$, that there would be an increase in the voltage output from the cell, which could also accelerate the evaporation of KOH.

5.3 Working During Covid

This year's MQPs faced a major challenge like no other year has before, which was dealing with the COVID-19 pandemic. The pandemic made on campus activities like classes and lab time difficult due to needing to get weekly testing and practicing social distancing. Lab time needed to be booked in advance and only two people were allowed in room GH221 at time and had to be distanced at least 6-feet apart. This made interactions between the group members extremely difficult and therefore made our time in the lab difficult. Furthermore, groups had limited access to resources and lab spaces to decrease the amount of potential contact with the virus. This cut off access to key resources such as the CV machine (cyclic voltammetry) which could have progressed this project further.

We also ran into issues when it came to our own health and wellness. Towards the end of B-term, one of the members of our group tested positive for COVID-19, forcing the whole group to go into immediate quarantine for two weeks. This cut off the time we had in the lab before winter break and the team felt we missed valuable lab time. However, this was essential to the health and safety of the rest of the WPI community and had to be done. Due to complications with the testing center, we also missed lab time during the winter break and had to rely on C-term and part of D-term to get the bulk of our testing done. Regular weekly testing still had to be done during these terms, but as time went on the group was able to grasp the new normal. We feel that we were able to complete a meaningful project even with the circumstances of the pandemic and the challenges that is brought.

6.0 Future Work

Despite having successful results which point to a flat and transparent configuration to be feasible, there is still many advancements that need to be addressed in future research and experimentation. First, materials such as the Zirconia cloth are only available for purchase through a certified buyer and may be difficult to obtain. We would suggest compiling a list of materials early so that materials are able to arrive sooner rather than later. On the topic of materials, the polyimide tape material used as the base for the configuration caused many issues throughout our experiments. Finding an alternative for this material may resolve issues such as KOH electrolyte leakage and permanent creases when being bent. Furthermore, gallium always had to be run in an incubator to stay around 50°C which then caused the electrolyte to evaporate. Looking further into the viability of using a gel electrolyte and galinstan in this cell could be a way to stabilize the cell and avoid issues like electrolyte leaking and evaporation. Due to the COVID-19 pandemic, our resources were limited, so utilizing resources like the cyclic voltammetry next year would help to better understand the internals of the configuration and to optimize the cell. Better understanding the chemistry and mechanics of this configuration will help with future research of liquid metal air batteries and bring them closer to commercial use which would change the dynamic of the battery market.

References

- [1] Hunt, Tam. “Is There Enough Lithium to Maintain the Growth of the Lithium-Ion Battery Market?” *Greentech Media*, Greentech Media, 6 Jan. 2020, www.greentechmedia.com/articles/read/is-there-enough-lithium-to-maintain-the-growth-of-the-lithium-ion-battery-m.
- [2] Vyas, Kashyap. “Can Lithium-Ion Batteries Change the World?” *Interesting Engineering*, Interesting Engineering, 25 Apr. 2019, interestingengineering.com/the-future-of-lithium-ion-batteries-can-they-really-change-the-world.
- [3] Salot, R., et al. “Microbattery Technology Overview and Associated Multilayer Encapsulation Process.” *Applied Surface Science*, vol. 256, no. 3, 2009, doi:10.1016/j.apsusc.2009.09.086.
- [4] Kjeang, Erik, et al. “Microfluidic Fuel Cells: A Review.” *Journal of Power Sources*, Elsevier, 17 Oct. 2008, www.sciencedirect.com/science/article/pii/S0378775308019186.
- [5] Lee, Jin Wook, et al. “Microfluidic Redox Battery.” *Lab on a Chip*, The Royal Society of Chemistry, 10 May 2013, pubs.rsc.org/en/content/articlehtml/2013/lc/c3lc50499a.
- [6] Liu, Qianfeng, et al. “Aqueous Metal-Air Batteries: Fundamentals and Applications.” *Energy Storage Materials*, Elsevier, 10 Dec. 2019, www.sciencedirect.com/science/article/abs/pii/S240582971931089X.
- [7] Daeneke, T., et al. “Liquid Metals: Fundamentals and Applications in Chemistry.” *Chemical Society Reviews*, The Royal Society of Chemistry, 3 Apr. 2018, pubs.rsc.org/en/content/articlepdf/2018/cs/c7cs00043j.
- [8] Bo, Guyue, et al. “Recent Progress on Liquid Metals and Their Applications.” *Advances in Physics: X*, vol. 3, no. 1, 2018, p. 1446359., doi:10.1080/23746149.2018.1446359.
- [9] Ding, Yu, et al. “Next-Generation Liquid Metal Batteries Based on the Chemistry of Fusible Alloys.” *ACS Central Science*, 2020, pubs.acs.org/doi/10.1021/acscentsci.0c00749.
- [10] Mendoza, N.F. “Flexible Battery Market to Hit \$500 Million in 2030.” *TechRepublic*, TechRepublic, 10 July 2020, www.techrepublic.com/article/flexible-battery-market-to-hit-500-million-in-2030/.
- [11] Fu, L, et al. “Design and Fabrication of a Micro Zinc/Air Battery.” *Journal of Physics: Conference Series*, vol. 34, 2006, pp. 800–805., doi:10.1088/1742-6596/34/1/132.
- [12] Garcia G, Schuhmann W, Ventosa E. A Three-Electrode, Battery-Type Swagelok Cell for the Evaluation of Secondary Alkaline Batteries: The Case of the Ni-Zn Battery. *ChemElectroChem*. 2016;3(4):592-597. doi:10.1002/celec.201500474

- [13] Zhang J, Zhou Q, Tang Y, Zhang L, Li Y. Zinc-air batteries: Are they ready for prime time? *Chem Sci.* 2019;10(39):8924-8929. doi:10.1039/c9sc04221k
- [14] Kim H, Boysen DA, Newhouse JM, et al. Liquid metal batteries: Past, present, and future. *Chem Rev.* 2013;113(3):2075-2099. doi:10.1021/cr300205k
- [15] Kelley DH, Weier T. Fluid Mechanics of Liquid Metal Batteries. *Appl Mech Rev.* 2018;70(2). doi:10.1115/1.4038699
- [16] Betts, A.G. *Making Aluminum*. 1 Aug. 1095.
- [17] Chen Z, Lee JB. Surface Modification with Gallium Coating as Nonwetting Surfaces for Gallium-Based Liquid Metal Droplet Manipulation. Published online 2019. doi:10.1021/acsami.9b12493
- [18] Majidi, Leily, et al. "Gallium-Based Room-Temperature Liquid Metals: Actuation and Manipulation of Droplets and Flows." *Frontiers: Mechanics of Materials*, Frontiers, 7 Aug. 2017, www.frontiersin.org/articles/10.3389/fmech.2017.00009/full.
- [19] R. C. Gough et al., "Self-Actuation of Liquid Metal via Redox Reaction," vol. 8, no. 1, pp. 6–10, Jan. 2016, doi: 10.1021/acsami.5b09466. [Online]. Available: <http://dx.doi.org/10.1021/acsami.5b09466>
- [20] Hu, V. W., Vu, H. B., & Zargorski, J. (2016) *Liquid Metal-Air Battery for Energy Storage*. : Worcester Polytechnic Institute.
- [21] Young, David A. "Phase Diagrams of the Elements." 1975, doi:10.2172/4010212.
- [22] Hong, Soon-Jik, and C. Suryanarayana. "Mechanism of Low-Temperature θ -CuGa₂ Phase Formation in Cu-Ga Alloys by Mechanical Alloying." *Journal of Applied Physics*, vol. 96, no. 11, 2004, pp. 6120–6126., doi:10.1063/1.1808243.
- [23] Kim, Yoonkap, and David F. Bahr. "Low Temperature Melting Point Metals for Hot MEMS Electrical Switching." *Washington State*, Washington State University, 2007, pp. 12–76.
- [24] Gadeau, R. A., 1936, "Refining of Aluminum," U.S. Patent No. 2,034,339.
- [25] Guarino, Ben. "Nobel Prize in Chemistry Awarded for Rechargeable Lithium-Ion Batteries." *The Washington Post*, WP Company, 18 Nov. 2019, www.washingtonpost.com/science/2019/10/09/nobel-prize-chemistry-awarded-lithium-ion-batteries/?CID=2019-XBU-Nobel-Batteries.
- [26] *Components of Cells and Batteries*, depts.washington.edu/matseed/batteries/MSE/components.html.

- [27] Liu, Zhao, et al. "The History of the Lithium-Ion Battery." *Accelerating Microscopy*, 11 Oct. 2019, www.thermofisher.com/blog/microscopy/the-history-of-the-lithium-ion-battery/.
- [28] Guarino, Ben. "Nobel Prize in Chemistry Awarded for Rechargeable Lithium-Ion Batteries." *The Washington Post*, WP Company, 18 Nov. 2019, www.washingtonpost.com/science/2019/10/09/nobel-prize-chemistry-awarded-lithium-ion-batteries/?CID=2019-XBU-Nobel-Batteries.
- [29] Liu G, Kim JY, Wang M, et al. Soft , Highly Elastic , and Discharge-Current-Controllable Eutectic Gallium – Indium Liquid Metal – Air Battery Operated at Room Temperature. 2018;1703652:1-9. doi:10.1002/aenm.201703652
- [30] Learning, Lumen. "Galvanic Cells: Chemistry for Majors." *Lumen*, OpenStax College, courses.lumenlearning.com/chemistryformajors/chapter/galvanic-cells/.
- [31] staff, Science X. "New Process Generates Hydrogen from Aluminum Alloy to Run Engines, Fuel Cells." *Phys.org*, Phys.org, 16 May 2007, phys.org/news/2007-05-hydrogen-aluminum-alloy-fuel-cells.html#:~:text=When%20aluminum%20atoms%20in%20the,producing%20hydrogen%20and%20aluminum%20oxide.&text=%22No%20toxic%20fumes%20are%20produced,recycled%20over%20and%20over%20again.
- [32] Jingxu Zheng, Tian Tang, Qing Zhao, Xiaotun Liu, Yue Deng, and Lynden A. Archer. "Physical Orphaning versus Chemical Instability: Is Dendritic Electrodeposition of Li Fatal?" 2019, 4 (6), 1349-1355. doi:10.1021/acsenergylett.9b00750
- [33] Reger, Daniel L. *Chemistry: Principles and Practice 3rd ed.*. Boston: Cengage Learning, 2010
- [34] Rapoza, K., & Marx, A. (2017). *Investigation of the Rechargeability of a Liquid Metal-Air Battery*. : Worcester Polytechnic Institute.
- [35] Athair, A., & Arnold, T. (2020). *Feasibility of Ambient Temperature Liquid Metal Air Batteries*. : Worcester Polytechnic Institute.

Appendix A: Noteworthy Videos

Video 1: Gough video



*Video 2: Gallium pulls away
from interface*



*Video 3: 4/1/21 discharge
(orphaning)*



Video 4: 3/30/21 Surface Test



***Video 5: Water Only Control
Test***



Appendix B: Incubator Setup

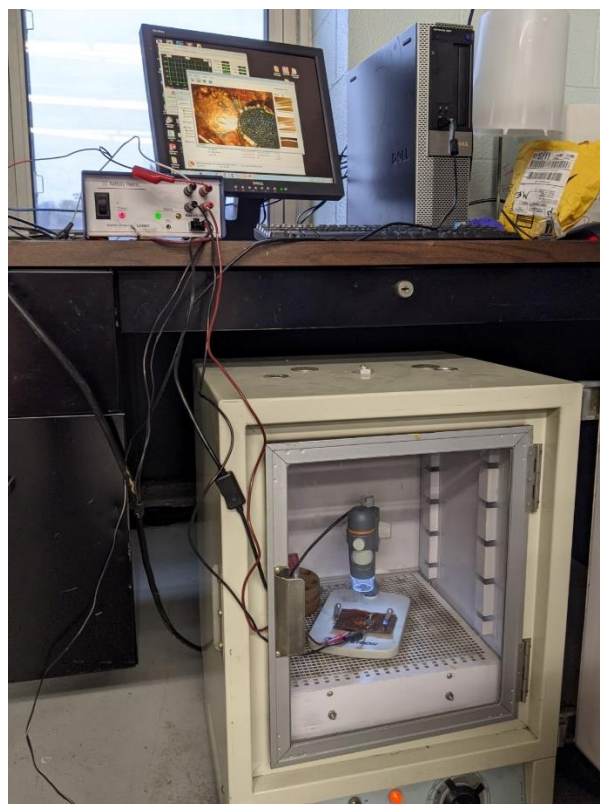


Figure 1A. *Incubator Lab Set-up to keep Gallium in liquid form. Incubator was always kept at 45°C. USB Microscope was able to function at the higher temperature.*

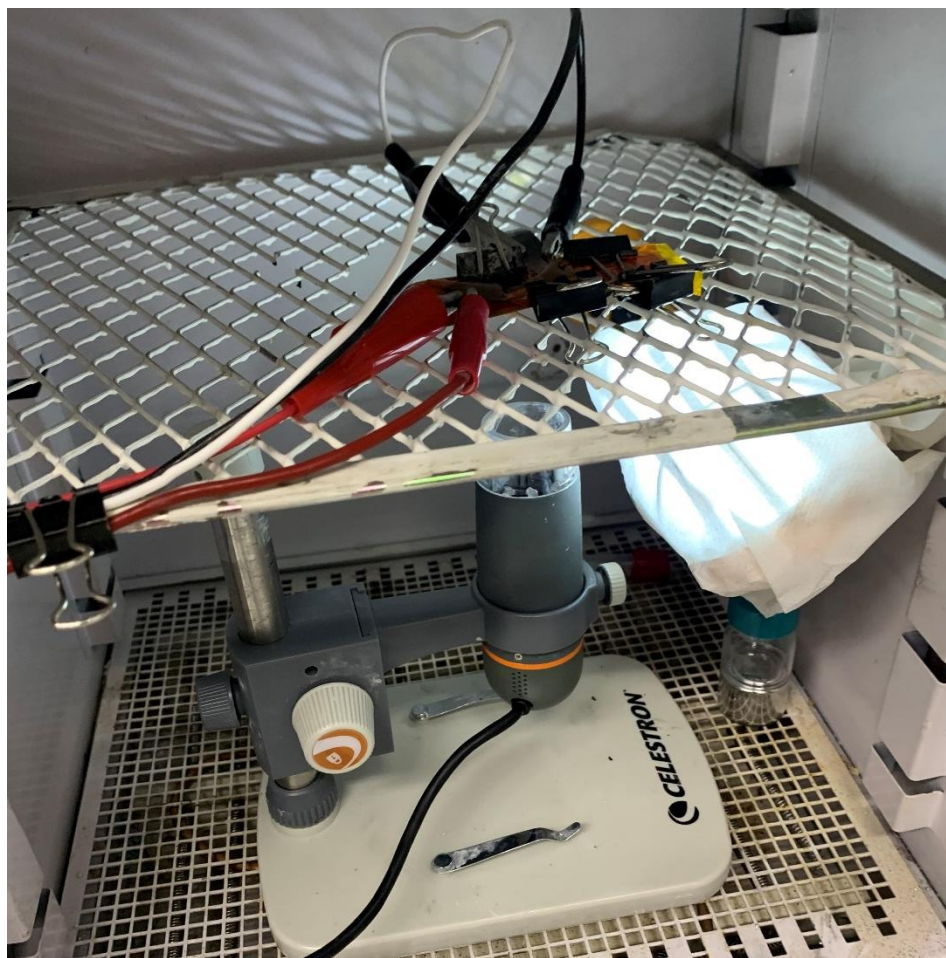


Figure 2A. *Module inside the incubator*

Appendix C: Assembling Gough Module



Figure 3A. *The Gough cell once we finished punching holes into the layers and stacking each layer including the silicon layer.*



Figure 4A. *We created many Gough cells at a time because of the leaking issues described above.*



Figure 5A. Shows the process of collecting the Galinstan into the syringe so that it be moved into the Gough cell's anode.



Figure 6A. Shows the process of placing the liquid Galinstan into the Gough cell through the silicon layer.

Appendix D: Miscellaneous Calculations

First Test

Before:

$$\text{Starting } pH = 7.3 \implies 7.3 = 14 - pOH \implies pOH = 6.7$$

$$pOH = -\log[OH^-] \implies 6.7 = -\log[OH^-] \implies [OH^-] = 1.995 \times 10^{-7} \frac{\text{moles}}{\text{liter}}$$

$$\text{Moles solute (n): } M = \frac{n}{v} \implies 1.995 \times 10^{-7} = \frac{n}{.022L} \implies n = 4.389 \times 10^{-9}$$

$$\# \text{ of particles: } (4.389 \times 10^{-9}) \times (6.02 \times 10^{23}) = 2.652 \times 10^{15}$$

After:

$$\text{After } pH = 9.69 \implies 9.69 = 14 - pOH \implies pOH = 4.31$$

$$pOH = -\log[OH^-] \implies 4.31 = -\log[OH^-] \implies [OH^-] = 4.897 \times 10^{-5} \frac{\text{moles}}{\text{liter}}$$

$$\text{Moles solute (n): } M = \frac{n}{v} \implies 4.897 \times 10^{-5} = \frac{n}{.022L} \implies n = 1.077 \times 10^{-6}$$

$$\# \text{ of particles: } (1.077 \times 10^{-6}) \times (6.02 \times 10^{23}) = 6.485 \times 10^{17} \text{ molecules}$$

Particle difference from before and after test:

$$(6.485 \times 10^{17}) - (2.652 \times 10^{15}) = 6.458 \times 10^{17} \text{ molecules}$$

$$\text{Calculated Current: } (6.458 \times 10^{17}) \times (1.6 \times 10^{-19}) = 103.3 \text{ mA}$$

Second Test

Before:

$$\text{Starting } pH = 7.4 \implies 7.4 = 14 - pOH \implies pOH = 6.6$$

$$pOH = -\log[OH^-] \implies 6.6 = -\log[OH^-] \implies [OH^-] = 2.512 \times 10^{-7} \frac{\text{moles}}{\text{liter}}$$

$$\text{Moles solute (n): } M = \frac{n}{v} \implies 2.512 \times 10^{-7} = \frac{n}{.022L} \implies n = 5.525 \times 10^{-9}$$

$$\# \text{ of particles: } (5.525 \times 10^{-9}) \times (6.02 \times 10^{23}) = 3.326 \times 10^{15}$$

After:

$$\text{After } pH = 8.42 \implies 8.42 = 14 - pOH \implies pOH = 5.58$$

$$pOH = -\log[OH^-] \implies 5.58 = -\log[OH^-] \implies [OH^-] = 2.63 \times 10^{-6} \frac{\text{moles}}{\text{liter}}$$

$$\text{Moles solute (n): } M = \frac{n}{v} \implies 2.63 \times 10^{-6} = \frac{n}{.022L} \implies n = 5.786 \times 10^{-8}$$

$$\# \text{ of particles: } (5.786 \times 10^{-8}) \times (6.02 \times 10^{23}) = 3.483 \times 10^{16} \text{ molecules}$$

Particle difference from before and after test:

$$(3.483 \times 10^{16}) - (3.326 \times 10^{15}) = 3.121 \times 10^{16} \text{ molecules}$$

$$\text{Calculated Current: } (3.121 \times 10^{16}) \times (1.6 \times 10^{-19}) = 4.99 \text{ mA}$$

Appendix E: Materials Purchased

Part Name:	Place of Purchase:	Model/ Part Number:
Polyimide Tape	Amazon.com	CECOMINOD047410
Hole Punch (3/8 in)	McMaster.com	3424A25
Galinstan – 50 grams	Rotometals.com	547825
Copper Foil Tape	McMaster.com	76555A721
Silicon Sheet	Amazon.com	B071KQLRXB
Acrylic Acid (for Gel Electrolyte)	Sigmaaldrich.com	MFCD00004367
K ₂ S ₂ O ₈ (for Gel Electrolyte)	Sigmaaldrich.com	MFCD00011386
N,N' -Methylenebisacrylamide (for Gel Electrolyte)	Sigmaaldrich.com	MFCD00008625
KOH	Sigmaaldrich.com	MFCD00003553
Gallium (50g, 99.99% pure)	Amazon.com	B07P7JN6VR
Platinum Catalyzed Carbon GDL	Pemeas Fuel Cell Technologies	LT40EW
Zirconia Separators	Zicarzirconia.com	(type ZYK-15)